Reconstructing Ocean pH with Boron Isotopes in Foraminifera

Gavin L. Foster[1] and James W.B. Rae[2]

[1]Ocean and Earth Science, National Oceanography Centre Southampton, University of Southampton, Waterfront Campus, Southampton SO14 3ZH, United Kingdom; email: glf1u08@soton.ac.uk

[2]Department of Earth and Environmental Sciences, University of St. Andrews, St. Andrews, Fife KY16 9AL, United Kingdom

Annu. Rev. Earth Planet. Sci. 2016. 44:207–37

First published online as a Review in Advance on April 27, 2016

The *Annual Review of Earth and Planetary Sciences* is online at earth.annualreviews.org

This article's doi: 10.1146/annurev-earth-060115-012226

Keywords

boron isotopes, pH, marine carbonates, pCO_2

Abstract

In order to better understand the effect of CO_2 on the Earth system in the future, geologists may look to CO_2-induced environmental change in Earth's past. Here we describe how CO_2 can be reconstructed using the boron isotopic composition ($\delta^{11}B$) of marine calcium carbonate. We review the chemical principles that underlie the proxy, summarize the available calibration data, and detail how boron isotopes can be used to estimate ocean pH and ultimately atmospheric CO_2 in the past. $\delta^{11}B$ in a variety of marine carbonates shows a coherent relationship with seawater pH, in broad agreement with simple models for this proxy. Offsets between measured and predicted $\delta^{11}B$ may in part be explained by physiological influences, though the exact mechanisms of boron incorporation into carbonate remain unknown. Despite these uncertainties, we demonstrate that $\delta^{11}B$ may provide crucial constraints on past ocean acidification and atmospheric CO_2.

1. INTRODUCTION

Boron is a volatile semimetallic element belonging to group 13 of the periodic table. It was first isolated in the early 1800s by Gay-Lussac & Thenard (1808) and is rarely found in nature as elemental B; instead, oxides and hydroxides dominate, with B commonly found in high concentrations in fluids as boric acid and in a number of minerals, such as colemanite ($CaB_3O_4(OH)_3 \cdot H_2O$) and borax ($Na_2(B_4O_5(OH)_4) \cdot 8H_2O$), which gives the element its name. Boron has relatively low concentrations in the bulk silicate Earth (~0.3 ppm) (McDonough & Sun 1995), but due to its incompatibility during mantle melting (similar to K) (McDonough & Sun 1995) and its ready solubility in fluids at moderate to high temperatures (≥100°C) (Leeman & Sisson 1996), it is concentrated in Earth's crust, with average upper crust being ~15 ppm B (Shaw et al. 1986, Leeman et al. 1992). The erosion of the upper crust is the primary source of B in the oceans (Lemarchand et al. 2002a), where it is a conservative element found in concentrations of ~4.5 ppm (Lee et al. 2010).

Boron has an atomic mass of 10.81, and it was first recognized by Aston (1920) that it has two stable isotopes: ^{10}B (~20%) and ^{11}B (~80%). Boron isotopic variation is reported using delta notation:

$$\delta^{11}B\,(‰) = \left(\left(\frac{^{11}B/^{10}B_{sample}}{^{11}B/^{10}B_{standard}}\right) - 1\right) \times 1{,}000, \quad (1)$$

where $^{11}B/^{10}B_{standard}$ is the boron isotopic composition of National Institute of Standards and Technology (NIST) Standard Reference Material (SRM) 951 boric acid ($^{11}B/^{10}B = 4.04367$) (Catanzaro et al. 1970). In many natural systems boron is bound to oxygen in either a tetrahedral complex, such as $B(OH)_4^-$ (borate ion), or a trigonal complex, such as $B(OH)_3$ (boric acid). Natural fractionation between the two isotopes is governed principally by their distribution between these complexes, with the ^{11}B incorporated preferentially in the more strongly bonded trigonal molecules. The fluid mobility of boron, the variability of boron speciation at low temperature, the relatively low mass of the element, and the large mass difference between its isotopes (~10%) all contribute to allow boron to exhibit a very large natural range of isotopic composition, from −30‰ to +50‰ (Barth 1993). As a result there is much interest in boron isotopic composition as a sensitive tracer of a variety of geochemical processes (e.g., Palmer & Swihart 1996).

In this review we focus on the growing use of the boron isotopic composition of marine carbonates, in foraminifera in particular, to trace ocean pH in the past (e.g., Sanyal et al. 1995; Pearson & Palmer 2000; Hönisch & Hemming 2005; Foster 2008; Hönisch et al. 2009; Pearson et al. 2009; Seki et al. 2010; Yu et al. 2010; Bartoli et al. 2011; Foster et al. 2012; Badger et al. 2013a,b; Foster & Sexton 2014; Greenop et al. 2014; Penman et al. 2014; Rae et al. 2014; Martínez-Botí et al. 2015a,b). Knowledge of past ocean pH allows reconstruction of CO_2 in the ancient atmosphere (e.g., Foster et al. 2012) and a greater understanding of why CO_2 changes (e.g., Rae et al. 2014), as well as documentation of the patterns and magnitude of ocean acidification (e.g., Penman et al. 2014).

The establishment of boron isotopes as a proxy for past pH has been made possible by a series of analytical developments in isotope geochemistry over the past 30 years. For instance, although the boron isotopic composition of natural materials had been measured for several decades (e.g., McMullen et al. 1961), it wasn't until the development of the very sensitive negative ion thermal ionization technique in the 1980s (measuring $^{10}B^{16}O_2^-$ and $^{11}B^{16}O_2^-$) (Zeininger & Heumann 1983) that the isotopic composition of the relatively small amounts of boron found in marine carbonates (3–50 ppm) (Vengosh et al. 1991, Hemming & Hanson 1992) could be precisely determined (Vengosh et al. 1991, Hemming & Hanson 1994). These measurements revealed that a variety of marine carbonates (foraminifera, pteropods, corals, ostracods) had $\delta^{11}B$ isotopically

lighter than seawater by 10–26‰ (Vengosh et al. 1991, Hemming & Hanson 1992). This light isotopic ratio was suggested to result from the preferential incorporation of borate ion into $CaCO_3$, and as the boron isotopic composition of this molecular species is pH dependent (see Section 3), it was recognized that the $\delta^{11}B$ of marine carbonates had the potential to trace ocean pH (Vengosh et al. 1991, Hemming & Hanson 1992, Spivack et al. 1993). However, despite this early promise, the application of the boron isotope pH proxy has, until recently, been limited by a number of challenges, including the accurate determination of the isotopic fractionation factor, constraints on incorporation mechanism, the influence of vital effects, and analytical uncertainty related to the difficulty of measuring the small amounts of boron found in marine carbonate. Significant advances have now been made on each of these fronts, allowing boron isotopes to be increasingly used to provide new insights into past changes in pH and CO_2. In this contribution we review the current understanding of the mechanics of the $\delta^{11}B$-pH proxy and its application to reconstructing ocean pH and atmospheric CO_2 in the past. As with most proxy systems, limitations and uncertainties remain, and the most important of these, as well as the outstanding challenges, are also discussed.

2. TRACING OCEAN pH AND ATMOSPHERIC CO_2 WITH BORON ISOTOPES

2.1. Why Do We Care About Ocean pH?

Between 1750 and 2015 humans released 590 Gt of CO_2. This has resulted in an increase in atmospheric CO_2 concentration of 120 ppm, so far driving global warming of ~1°C. At the same time the oceans have taken up roughly a third of the CO_2 emitted (Khatiwala et al. 2013), and as CO_2 is a weak acid, this has lowered surface ocean pH by 0.1 pH units (a 26% increase in $[H^+]$). This paired CO_2-driven climate change and ocean acidification is likely to have significant impact on land and marine ecosystems and the human civilizations that depend on them (e.g., Ciais et al. 2013, Gattuso et al. 2015), and it is thus a major goal of science and society to better understand how the Earth system responds to changes in CO_2. One way this can be achieved is by reconstructing changes in CO_2 and pH in the geological past (e.g., Rohling et al. 2012).

To understand changes in past ocean acidification and atmospheric CO_2, we must begin by considering the behavior of CO_2 in the ocean. This is crucial because the ocean contains around 60 times more CO_2 than the atmosphere and, unlike geological carbon reservoirs, can exchange this CO_2 with the atmosphere on decadal to millennial timescales (Holmen 1992). The abundance of CO_2 in seawater, compared with most other gases, is the result of the reaction of CO_2 and water to form carbonic acid, bicarbonate, and carbonate ion via the following reactions:

$$CO_2 + H_2O \overset{K_1}{\Leftrightarrow} H^+ + HCO_3^{2-} \overset{K_2}{\Leftrightarrow} 2H^+ + CO_3^{2-}, \quad (2)$$

where K_1 and K_2 are the first and second dissociation constants for carbonic acid in seawater. The sum of the carbon-containing molecules in Equation 2 is known as total CO_2 or dissolved inorganic carbon (DIC). The extent to which this system of weak acids is dissociated results from the need to balance the sum of the charges on the strong acids and bases in seawater, a property equivalent to seawater alkalinity (ALK). If alkalinity is large and the pool of DIC to balance it is relatively small, then the DIC will be pulled toward the charged bicarbonate and carbonate species; vice versa, if a large pool of DIC exists but alkalinity is small, much of the DIC must be present as uncharged CO_2. Like CO_2, ocean pH is primarily controlled by the balance of alkalinity and DIC, and pH and CO_2 are thus tightly coupled (**Figure 1**).

The quantitative relationship between pH and CO_2 is described by the ocean carbonate system. This is made up of six key variables (pH, CO_2 (aq), DIC, ALK, CO_3^{2-}, and HCO_3^{2-}), related to

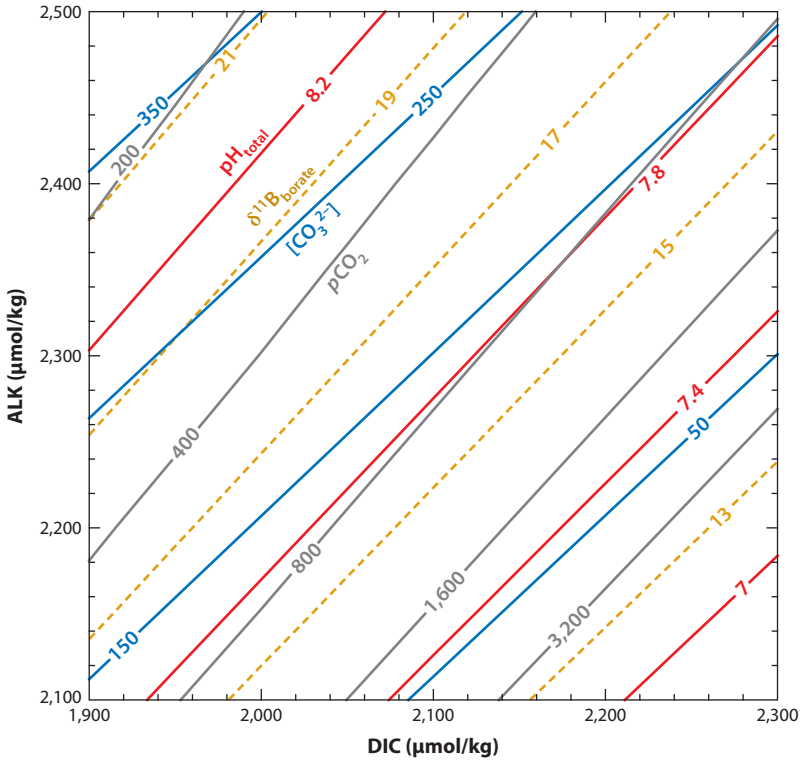

Figure 1

Seawater pH (total scale, *red*; pCO_2, *gray*; $[CO_3^{2-}]$, *blue*; $\delta^{11}B_{borate}$, *dashed orange*) as a function of alkalinity (ALK) and dissolved inorganic carbon (DIC).

one another by the following four equations:

$$\mathrm{DIC} = [\mathrm{CO_2}] + [\mathrm{HCO_3^-}] + [\mathrm{CO_3^{2-}}], \tag{3}$$

$$\mathrm{ALK} = [\mathrm{HCO_3^-}] + 2\,[\mathrm{CO_3^{2-}}] - [\mathrm{H^+}], \tag{4}$$

$$K_1^* = \frac{[\mathrm{HCO_3^-}][\mathrm{H^+}]}{[\mathrm{CO_2}]}, \tag{5}$$

$$K_2^* = \frac{[\mathrm{CO_3^{2-}}][\mathrm{H^+}]}{[\mathrm{HCO_3^-}]}. \tag{6}$$

The oceanic carbonate system thus has two degrees of freedom, so knowledge of pH and one other carbonate system variable allows for the full quantification of the system (though note that K_1^* and K_2^* are temperature, salinity, and pressure dependent, so these state variables must also be known). Although the full expression for ocean alkalinity includes other minor weak acids and bases, these variables are added to the system along with independent equations such that the carbonate system always has two degrees of freedom. Quantification of $[CO_2]$ allows us to

calculate the concentration of atmospheric CO_2 in equilibrium with this water via Henry's law:

$$CO_2(g) \overset{K_0}{\Leftrightarrow} CO_2(aq), \tag{7}$$

where K_0 is the solubility coefficient of CO_2 in seawater, allowing quantitative constraints to be placed on atmospheric CO_2 in the past based principally on a paleorecord of surface ocean pH. A growing number of studies have thus used pH records from boron isotopes to reconstruct past atmospheric CO_2 (e.g., Sanyal et al. 1995, Pearson & Palmer 2000, Hönisch et al. 2009, Pearson et al. 2009, Seki et al. 2010, Foster et al. 2012, Martínez-Botí et al. 2015a); others have investigated how the oceans have driven changes in atmospheric CO_2 over the Quaternary (e.g., Yu et al. 2013; Rae et al. 2014; Martínez-Botí et al. 2015a,b), whereas still others have traced the magnitude of oceanic uptake of anthropogenic CO_2 over the past 200 years (Liu et al. 2014). In short, it is the close link between pH and oceanic and atmospheric CO_2 that makes a proxy for past ocean pH of great interest in the geosciences.

2.2. The Boron Isotope pH Meter

The ability of boron isotopes in carbonates to record past pH stems from the acid-base chemistry of boron in seawater. Boron exists in seawater predominantly in two forms, boric acid ($B(OH)_3$) and borate ion ($B(OH)_4^-$), with the total concentration of boron in seawater denoted as $[B]_{sw}$:

$$[B]_{sw} = [B(OH)_3] + [B(OH)_4^-]. \tag{8}$$

These molecules are related by the following acid-base equilibrium:

$$B(OH)_3 + H_2O \Leftrightarrow B(OH)_4^- + H^+. \tag{9}$$

The stoichiometric equilibrium constant (K_B^*) of this reaction is

$$K_B^* = \frac{[B(OH)_4^-][H^+]}{[B(OH)_3]}, \tag{10}$$

with a value of $\sim 10^{-8.6}$ (or $pK_B^* \approx 8.6$) in seawater at 25°C, 35 psu, and atmospheric pressure (note that the influence of temperature, salinity, and pressure on K_B^* is relatively minor and well constrained) (**Figure 2**) (Dickson 1990). As pK_B^* is close to typical seawater pH (~8), the concentrations of $B(OH)_3$ and $B(OH)_4^-$ vary considerably with ocean pH (**Figure 3*a***):

$$[B(OH)_3] = \frac{[B]_{sw}}{1 + K_B^*/[H^+]}, \tag{11}$$

$$[B(OH)_4^-] = \frac{[B]_{sw}}{1 + [H^+]/K_B^*}. \tag{12}$$

Although the distribution of boron in seawater between $B(OH)_3$ and $B(OH)_4^-$ varies, the behavior of total boron in seawater ($[B]_{sw}$) is conservative, with a concentration given by (Lee et al. 2010):

$$[B]_{sw} = 432.6 \frac{\mu mol}{kg} \times \frac{salinity}{35}. \tag{13}$$

The isotopic composition of total boron in seawater ($\delta^{11}B_{sw}$) is 39.61‰ (Foster et al. 2010), and this is invariant on multi-million-year timescales, due to boron's long residence time (10–20 Myr) (Lemarchand et al. 2002a).

Due to differences in coordination and vibrational frequency there is a pronounced isotopic fractionation between $B(OH)_3$ and $B(OH)_4^-$, with ^{11}B preferentially incorporated into boric acid.

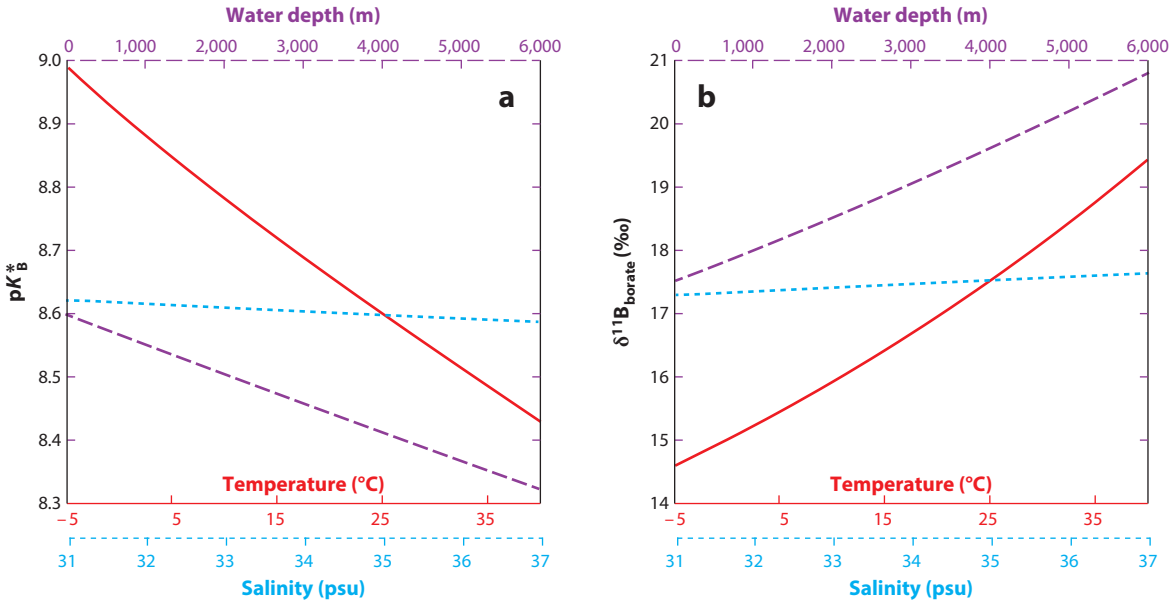

Figure 2

(*a*) The influence of temperature (*red*), salinity (*light blue*), and water depth (i.e., pressure; *purple*) on the dissociation of boric acid (pK_B^*). Note that temperature has the largest effect on pK_B^*. (*b*) The influence of temperature, salinity, and pressure on the $\delta^{11}B$ of borate ion at a constant pH of 8.0, due to the changes in pK_B^* shown in panel *a*.

The isotopic exchange between these species can be described by the reaction

$$^{10}B(OH)_3 + {}^{11}B(OH)_4^- \Leftrightarrow {}^{11}B(OH)_3 + {}^{10}B(OH)_4^-, \quad (14)$$

with the isotopic fractionation, α_B (also written $^{11-10}K_B$ and α_{B4-3}), given as

$$\alpha_B = \frac{{}^{\frac{11}{10}}R_{B(OH)_3}}{{}^{\frac{11}{10}}R_{B(OH)_4^-}}, \quad (15)$$

where ${}^{\frac{11}{10}}R$ is the $^{11}B/^{10}B$ ratio of each species. The fractionation factor is also commonly expressed in epsilon units:

$$\varepsilon_B = (\alpha_B - 1) \times 1{,}000. \quad (16)$$

Given the isotopic fractionation between the boron species, and the fact that their abundance changes with pH yet must sum to give $[B]_{sw}$ and $\delta^{11}B_{sw}$, it follows that the isotopic composition of each species will vary as a function of pH (**Figure 3*b***). In simplified form, this can be represented by the following mass balance equation:

$${}^{\frac{11}{10}}R_{B_{sw}} \times [B]_{sw} = {}^{\frac{11}{10}}R_{B(OH)_3} \times [B(OH)_3] + {}^{\frac{11}{10}}R_{B(OH)_4^-} \times [B(OH)_4^-]. \quad (17)$$

For instance, at pH < 7, the majority of the boron in seawater is in the boric acid form (**Figure 3**), so boric acid must have a $\delta^{11}B$ equal to $\delta^{11}B_{sw}$ (i.e., 39.61‰), and an infinitesimal amount of borate will be present, with a $\delta^{11}B$ offset below boric acid by a function of α_B. Similarly, at pH > 10, the majority of boron is present as borate ion, which must therefore have the $\delta^{11}B$ of total boron in seawater, while an infinitesimal amount of boric acid will be present, with elevated $\delta^{11}B$ (**Figure 3**). The isotopic composition of either molecule may be calculated by rearranging the

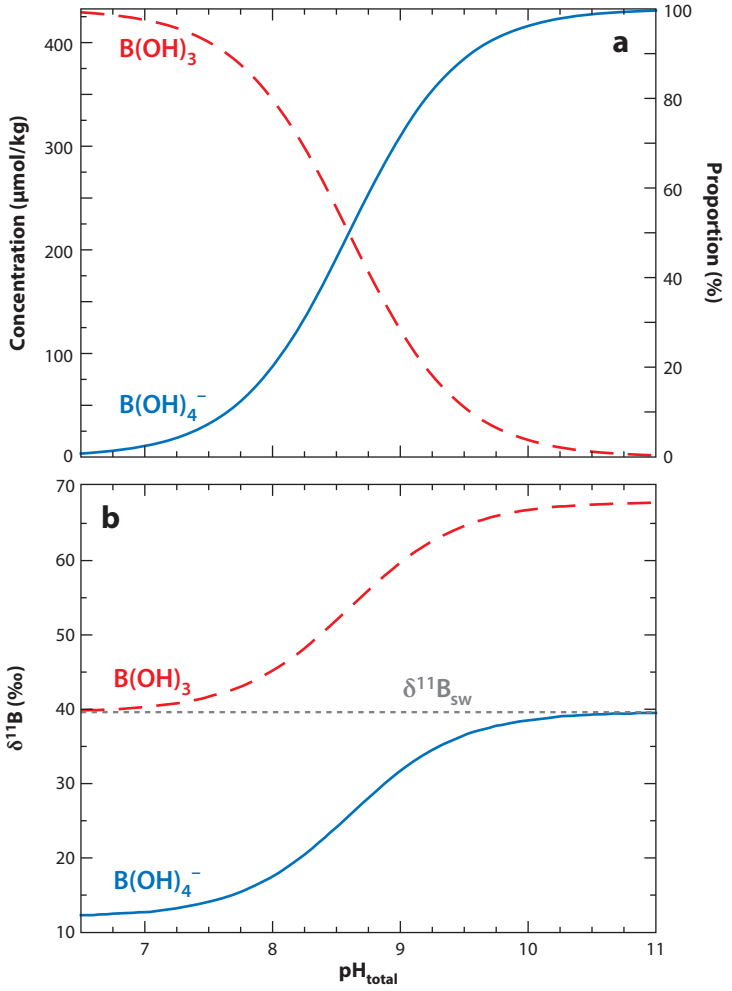

Figure 3

Variation in (*a*) concentration and (*b*) isotopic composition of borate ion ($B(OH)_4^-$) and boric acid ($B(OH)_3$) with seawater pH (total scale). Graphs are plotted for standard surface seawater conditions, with temperature of 25°C and salinity of 34.7 psu, giving $pK_B^* \approx 8.6$, and with $\alpha_B = 1.0272$ (Klochko et al. 2006), isotopic composition of boron in seawater ($\delta^{11}B_{sw}$) = 39.61‰ (Foster et al. 2010), and total boron in seawater ($[B]_{sw}$) = 432.6 × (salinity/35) μmol/kg (Lee et al. 2010). Note that different temperature, salinity, and pressure conditions lead to different pK_B^* values, giving subtle differences in the trends plotted here (see **Figure 2**).

mass balance in Equation 17 and substituting in Equation 15:

$$^{11}_{10}R_{B(OH)_4^-} = \frac{^{11}_{10}R_{B_{sw}} \times [B]_{sw}}{[B(OH)_4^-] + \alpha_B[B(OH)_3]}. \quad (18)$$

This may be converted to delta notation by substituting Equations 1, 8, and 16 to give

$$\delta^{11}B_{B(OH)_4^-} = \frac{\delta^{11}B_{sw}[B]_{sw} - \varepsilon_B[B(OH)_3]}{[B(OH)_4^-] + \alpha_B[B(OH)_3]}, \quad (19)$$

$$\delta^{11}B_{B(OH)_3} = \delta^{11}B_{B(OH)_4^-} \times \alpha_B + \varepsilon_B. \quad (20)$$

Because the dominant control on the concentration of each species in seawater is pH, the $\delta^{11}B$ of each species is a close and easily described function of pH (**Figure 3**); for example,

$$\delta^{11}B_{B(OH)_4^-} = \frac{\delta^{11}B_{sw} + (\delta^{11}B_{sw} - \varepsilon_B) \times 10^{pK_B^* - pH}}{1 + \alpha_B \times 10^{pK_B^* - pH}}. \quad (21)$$

As K_B^* is a function of temperature, pressure, and salinity, the $\delta^{11}B$ of each species also varies with these environmental conditions (**Figure 2**), albeit with a reduced sensitivity compared with pH. For instance, at atmospheric pressure, 25°C, and 35 psu, a pH increase from 8.2 to 8.3 causes the $\delta^{11}B$ of borate to increase by 1.34‰, whereas increasing temperature by 1°C and salinity by 1 psu at pH 8.2 changes the $\delta^{11}B$ of borate by 0.15‰ and 0.07‰, respectively (**Figure 2**).

As the isotopic compositions of borate and boric acid are functions of pH, it follows that if we could reconstruct the $\delta^{11}B$ of one of these molecules in the past, we could reconstruct pH. In short, this is made possible by the inference that it is predominantly the borate molecule that is incorporated into marine carbonates (Hemming & Hanson 1992). This allows us to use the homogeneous equilibrium of boron and its isotopes in solution as described above, along with measurements of $\delta^{11}B$ in marine carbonates, to reconstruct the pH of the seawater in which the carbonate precipitated. The details of boron isotopes in carbonates and their measurement, incorporation, and application to reconstruct pH and CO_2 are discussed in detail in Sections 3 and 4, and are now the major areas of research on the $\delta^{11}B$-pH proxy. However, before leaving this underlying solution chemistry behind, we review the substantial body of work on the determination of the isotopic fractionation factor α_B.

There have been numerous attempts to determine the value of α_B in seawater, with the majority relying on either empirical methods or ab initio calculations (e.g., Kakihana et al. 1977, Hemming et al. 1995, Oi 2000, Liu & Tossell 2005, Pagani et al. 2005, Sanchez-Valle et al. 2005, Zeebe 2005, Klochko et al. 2006, Rustad et al. 2010). Klochko et al. (2006) presented the first direct measurement of α_B in seawater and determined it to be 1.0272 ± 0.0006 at 25°C and a salinity of 35 psu. Although a widely used earlier calculation based on vibrational frequency data suggested a lower value (1.0194) (Kakihana & Kotaka 1977, Kotaka & Kakihana 1977), Rustad & Bylaska (2007) showed these calculations were erroneous due to the misassignment of a major vibrational mode. More recent studies based on theoretical considerations give higher values, largely consistent with the measurements of Klochko et al. (2006) (~1.025–1.035) (Oi 2000, Liu & Tossell 2005, Zeebe 2005, Rustad et al. 2010). A recent independent method, which used a novel reverse osmosis approach to separate and then measure the isotopic composition of the boric acid species in seawater, determined $\alpha_B = 1.0260 \pm 0.0010$ (Nir et al. 2015), within error of Klochko et al.'s (2006) value.

Theoretical constraints suggest α_B should also vary as a function of temperature (e.g., Kakihana et al. 1977), but the calculated size of this sensitivity is highly uncertain (Zeebe 2005). Klochko et al. (2006) performed measurements of α_B at elevated temperature (40°C) in seawater, giving 1.0269 ± 0.0027, within error of the value for 25°C but with relatively large uncertainty. As a result, the environmental sensitivity of α_B is currently underconstrained.

Given the multitude of other controlling influences (see Section 4), it is difficult to isolate the sensitivity of α_B to other secondary environmental variables using empirical studies of $\delta^{11}B$ in $CaCO_3$ (of either inorganic or biogenic origin). Nonetheless, the majority of empirical studies examining $\delta^{11}B$ in modern biogenic $CaCO_3$ suggest that within the temperature range of 2–30°C, any change in α_B is likely insignificant relative to the other uncertainties involved in $\delta^{11}B$-pH calibrations (i.e., is likely less than analytical precision, <0.2‰) and can effectively be ignored

(Rae et al. 2011, Henehan et al. 2013). One study (Dissard et al. 2012) reported a temperature sensitivity of $\delta^{11}B$ in the coral *Acropora* sp. of ~0.15‰ per °C when grown at pH of 8.015, salinity of 38 psu, and temperatures from 22°C to 28°C. However, this apparent sensitivity is most likely due to change in K_B^* as temperature increases, which the authors did not consider. For example, from 22°C to 28°C we would expect the $\delta^{11}B$ of $B(OH)_4^-$ to increase by ~0.13‰ per °C, similar to Dissard et al.'s (2012) observations.

2.3. Isotopic Analysis of Boron in Marine Carbonates

As outlined above, there is a strong theoretical basis for the $\delta^{11}B$-pH proxy. However, the boron isotopic composition of marine carbonates is notoriously difficult to measure accurately. As a light isotope system, the relative mass difference between ^{10}B and ^{11}B is large (~10%), giving large potential isotopic fractionations during chemical processing and measurement. Therefore, a major difficulty arises from the need to accurately control and correct analytical fractionations. Furthermore, the quantity of boron available in typical marine carbonate samples is small (~2–20 ng), so analytical techniques must be sensitive and efficient, and laboratory contamination must be carefully controlled and minimized. Finally, given the relatively small oceanographic changes in past pH that we hope to reconstruct (typically equivalent to <1‰), techniques must be both accurate and precise.

The first high-precision boron isotope measurements on natural materials were made by positive thermal ionization mass spectrometry (PTIMS) (e.g., Ramakumar et al. 1985, Swihart 1996, Lemarchand et al. 2002b). As the ionization potential of boron is extremely high, analysis is carried out as an alkali-borate complex. Early studies used sodium as an activator (giving $Na_2BO_2^+$ beams) (Swihart et al. 1986) and achieved precision of around ±2‰ (2 SD). Precision was improved to around ±0.4‰ by using cesium ($Cs_2BO_2^+$ beams) (Ramakumar et al. 1985), with the small relative mass difference between the heavy 308 and 309 amu $Cs_2BO_2^+$ beams minimizing instrumental mass fractionation. However, most applications of this technique require a large mass of boron (~1,000 ng), substantially greater than what is available for many marine carbonate samples (10–20 ng). Although some recent studies have managed to reduce these sample size requirements (~25 ng) (He et al. 2013a) and applied PTIMS $\delta^{11}B$ measurements to corals (Liu et al. 2009, Trotter et al. 2011), PTIMS measurements remain uncommon in the application of $\delta^{11}B$ to study past changes in the ocean carbonate system.

To improve sensitivity and reduce sample size requirements for boron, negative thermal ionization mass spectrometry (NTIMS) techniques were developed (Zeininger & Heumann 1983, Vengosh et al. 1989, Hemming & Hanson 1994). This method analyses boron as BO_2^- beams, produced using either dissolved calcium carbonate or boron-free seawater as an activator. The technique is extremely sensitive, with small (<1 ng) boron samples producing large (up to ~20 V) $^{11}BO_2^-$ beams lasting for several hours (Hemming & Hanson 1994). The major challenge of this technique, as with any dual isotope system measured by TIMS, is to accurately account for instrumental mass fractionation (also known as mass bias). This is a particular concern given the difference in ionization behavior between carbonate samples, which are dissolved and loaded directly onto filaments, and standards, typically NIST SRM 951 loaded in boron-free artificial seawater. Despite these difficulties, reliable data can be generated provided strict analytical protocols are followed (e.g., see Hemming & Hönisch 2007, Foster et al. 2013).

With the advent (Walder & Freedman 1992) and proliferation (e.g., Halliday et al. 1998) of multicollector inductively coupled plasma mass spectrometry (MC-ICPMS), it was soon recognized that the major limitation of the TIMS analysis of dual isotope systems (i.e., the difficulty of correcting for mass bias) could be overcome with this new technology, and early applications to

boron met with some success (e.g., Lecuyer et al. 2002, Aggarwal et al. 2003). Improved analytical sensitivity with later generations of MC-ICPMS has led to the rapid expansion of this technique for determining the boron isotopic composition of marine carbonates (Foster 2008, Louvat et al. 2010, Guerrot et al. 2011, McCulloch et al. 2014).

Despite the success of MC-ICPMS analyses, some challenges do remain. Chief among these are the difficulties associated with chemical purification of boron. This is typically done using column chromatography, often taking advantage of the boron-specific resin Amberlite IRA 743 (Kiss 1988). More recently, microsublimation techniques have been attempted with some success for coral samples (e.g., Liu et al. 2014), but this approach also requires significant operator skill (Wang et al. 2010), and recent work shows reproducibility of ~1.8‰ on solid splits of the same foraminiferal sample (Misra et al. 2014). This may suggest variable mass fractionation during sublimation in subtly different matrices. Methods using column chromatography seem more reliable (<0.25‰) (Foster 2008, Louvat et al. 2010, Foster et al. 2013), but the extra sample handling means laboratory blanks must be well controlled.

Alongside the expansion of boron isotope analyses, the boron isotope community has adopted reference materials to assist in interlaboratory comparison. For instance, the Japanese Geological Survey coral (JcP-1) reference material is now routinely reported by laboratories, with a good level of interlaboratory agreement (published estimates typically range from 24.2‰ to 24.4‰) (Wang et al. 2010, Dissard et al. 2012, Henehan et al. 2013, Liu et al. 2014, McCulloch et al. 2014). Despite the difficulties associated with chemical purification and analysis of boron (e.g., see Foster et al. 2013 for more discussion), these recent developments in boron isotope analysis by MC-ICPMS have considerably broadened the utility of the δ^{11}B-pH proxy.

3. BORON ISOTOPIC COMPOSITION OF MARINE CARBONATES: THEORY

Hemming & Hanson (1992) proposed the first model for boron incorporation into $CaCO_3$, based principally on the observation that the δ^{11}B of marine carbonates is similar to the δ^{11}B of seawater $B(OH)_4^-$. Although constructed using a limited data set for δ^{11}B and [B] of biogenic $CaCO_3$, it has proved to be remarkably resilient, and although we are now aware of various other considerations, it still forms the basis of the δ^{11}B-pH proxy.

Central to the Hemming & Hanson (1992) model is the suggestion that only the charged species, borate ion, is attracted to the growing surface of a calcite or aragonite crystal. They reasoned, based on measured δ^{11}B, that borate is structurally incorporated into the $CaCO_3$ and, given that the B–O bond length is similar to the C–O bond length (Kakihana et al. 1977), that borate ion substitutes for carbonate ion (CO_3^{2-}) via the following reaction:

$$CaCO_3 + B(OH)_4^- \Rightarrow Ca(HBO_3) + HCO_3^- + H_2O. \quad (22)$$

HBO_3^{2-} was suggested as the species incorporated into the trigonal calcite lattice because of its similarity in terms of both size and charge to CO_3^{2-}. This requires a change in coordination of the boron from tetrahedrally coordinated $B(OH)_4^-$ to trigonally coordinated HBO_3^{2-}, which Hemming & Hanson (1992) assumed occurs without additional isotopic fractionation. These authors also suggested that tetrahedral $B(OH)_4^-$ might be directly incorporated into the tetrahedral aragonite lattice, perhaps explaining the higher boron concentrations typically found in this polymorph (Hemming et al. 1995, 1998).

Combined with the recent constraints on α_B described above, this model allows pH to be determined from the δ^{11}B of a marine carbonate ($\delta^{11}B_{CaCO_3}$) using the following equation (from

Zeebe & Wolf-Gladrow 2001):

$$\mathrm{pH} = \mathrm{p}K_B^* - \log\left(-\frac{\delta^{11}B_{sw} - \delta^{11}B_{CaCO_3}}{\delta^{11}B_{sw} - \alpha_B\delta^{11}B_{CaCO_3} - \varepsilon_B}\right). \quad (23)$$

Provided $\delta^{11}B_{sw}$ is known, and temperature, pressure, and salinity are constrained such that K_B^* can be accurately determined, the $\delta^{11}B$ of $CaCO_3$ should be a sensitive tracer of the pH of the fluid in which the $CaCO_3$ grew.

The Hemming & Hanson (1992) model of boron incorporation also suggests that the concentration of boron in $CaCO_3$ should reflect the abundance of aqueous $B(OH)_4^-$ and HCO_3^-. A distribution coefficient can be defined for the substitution reaction above, as

$$K_D = \frac{[B/Ca]_{CaCO_3}}{[B(OH)_4^-/HCO_3^-]_{aq}}. \quad (24)$$

The boron content of $CaCO_3$ can thus be described by

$$[B/Ca]_{CaCO_3} = K_D \times [B(OH)_4^-/HCO_3^-]_{aq}, \quad (25)$$

with $[B(OH)_4^-/HCO_3^-]_{aq}$ being a function of pH (Yu & Elderfield 2008).

4. BORON ISOTOPIC COMPOSITION OF MARINE CARBONATES: REALITY

The inorganic model for $\delta^{11}B$ in carbonates described above has now been tested on a variety of types of marine carbonates. Inorganic $CaCO_3$ precipitates have the advantage of avoiding physiological influences, but despite recent progress (Noireaux et al. 2015), these studies remain limited in number and scope (e.g., growth in low-ionic-strength media). Studies based on biogenic carbonates must take potential physiological influences into account when seeking to understand the systematics of boron incorporation, but provide a more direct calibration for pH and CO_2 reconstructions using the fossil record. Below we describe $\delta^{11}B$ in a range of available carbonate types, with a focus on foraminifera.

Figure 4 shows a selection of published $\delta^{11}B$ data for carbonates grown at known pH and measured in a variety of laboratories using several analytical techniques. Because of the environmental sensitivity of K_B^* (**Figure 2**), it is not straightforward to compare different culture studies and field calibrations on the same $\delta^{11}B$-pH plot. Instead, it has been proposed (Foster 2008, Rae et al. 2011, Henehan et al. 2013) that plots of aqueous $\delta^{11}B_{borate}$ (at in situ conditions) and measured $\delta^{11}B_{CaCO_3}$ should be used to compare between studies (**Figure 5**). The gradients and intercepts of the carbonate data on such plots are independent of K_B^* (and hence salinity, temperature, and pressure), meaning that different calibration studies can be readily compared without reference to in situ environmental conditions. Any difference in gradient on such a plot indicates a different pH sensitivity of $\delta^{11}B_{CaCO_3}$ compared to $\delta^{11}B_{borate}$ (i.e., a different curvature of the $\delta^{11}B$-pH relationship). As we will see later, such a method also allows for easier treatment of $\delta^{11}B$-pH calibrations.

Calibration data show that $\delta^{11}B$ of marine $CaCO_3$ is typically a well-defined function of seawater pH (**Figures 4** and **5**). As a result, $\delta^{11}B$ can be used to reconstruct past pH to a high fidelity provided it is empirically calibrated for the species of interest. However, a feature common to all but the calcitic benthic foraminifera measured by MC-ICPMS by Rae et al. (2011) is that, despite a strong pH dependency, $\delta^{11}B_{CaCO_3}$ is offset from $\delta^{11}B_{borate}$ (**Figures 4** and **5**). In the following sections a number of possible reasons for offsets between $\delta^{11}B_{CaCO_3}$ and $\delta^{11}B_{borate}$ are discussed.

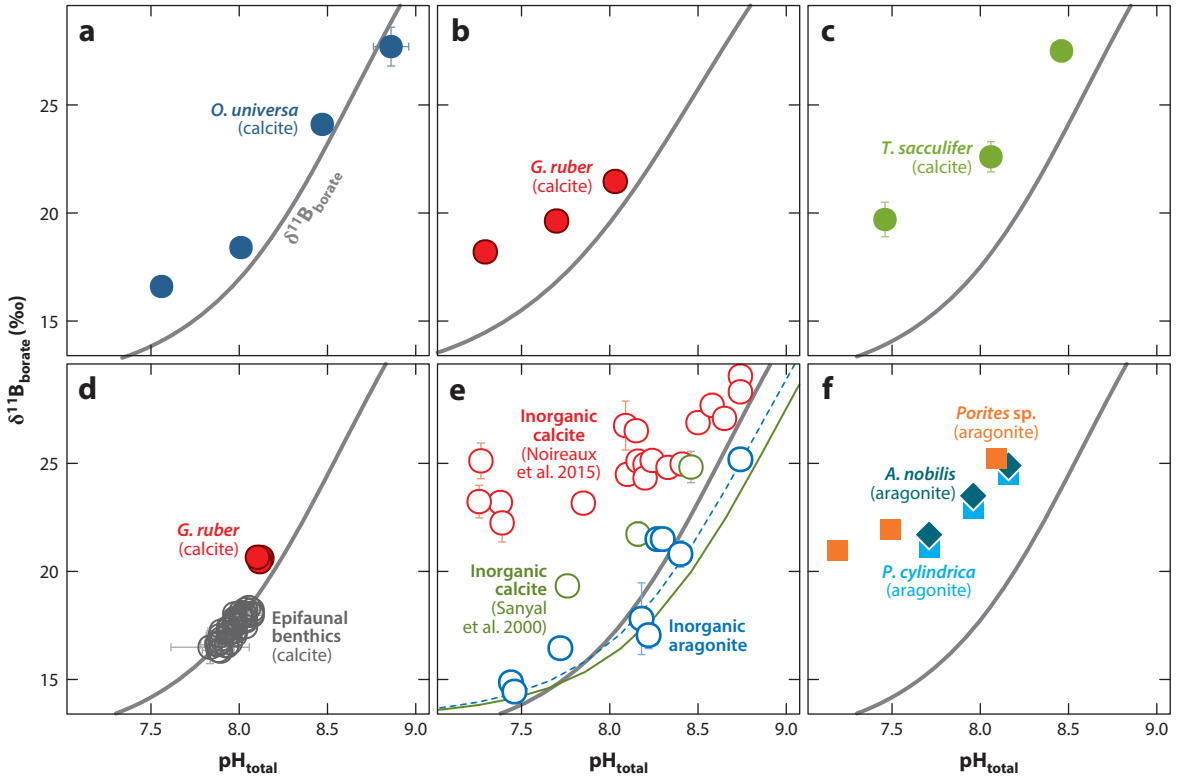

Figure 4

The boron isotopic composition of (*a–d*) low-Mg calcite foraminifera, (*e*) inorganic $CaCO_3$, and (*f*) scleractinian coral aragonite, compared to the pH of the water in which they grew; all except the inorganic data from Noireaux et al. (2015) are on the total pH scale. (*a*) Cultured planktic foraminifera *Orbulina universa* from Sanyal et al. (1996). (*b*) Cultured planktic foraminifera *Globigerinoides ruber* from Henehan et al. (2013). (*c*) Cultured planktic foraminifera *Trilobatus sacculifer* from Sanyal et al. (2001). (*d*) Core top epifaunal benthic foraminifera (*dark gray open circles*) from Rae et al. (2011), including *Cibicidoides wuellerstorfi*, *Cibicidoides mundulus*, and *Planulina arimiensis*. Also shown, in red, are the core top planktic foraminifera *G. ruber* data from Foster (2008). In both cases the $\delta^{11}B$ has been corrected to a constant pK_B^* as detailed in Henehan et al. (2013). (*e*) Inorganically grown calcite from Sanyal et al. (2000) (*green open circles*) and from Noireaux et al. (2015) (*red open circles*). Inorganic aragonite from Noireaux et al. (2015) (*blue open circles*). (*f*) Cultured corals *Acropora nobilis* and *Porites cylindrica* from Hönisch et al. (2004) and *Porites* sp. from Krief et al. (2010). In all plots the thick solid gray line is the $\delta^{11}B$ of borate calculated at culture/controlled conditions. For panels *a*, *c*, and *e*, corrections were made to place the data on the total pH scale ($pH_{total} = pH_{NBS} - 0.14$), and for $\delta^{11}B_{borate}$ in panel *a* and Sanyal et al.'s (2000) data in panel *e*, temperature and salinity were assumed to be 20°C and 35 psu, respectively. In panel *e*, the inorganic $CaCO_3$ data from Noireaux et al. (2015) were obtained in low-ionic-strength $Na(Ca)Cl_2$, and the blue dashed (for aragonite) and green solid (for calcite) lines reflect the appropriate $\delta^{11}B_{borate}$ in these nonseawater growth media. Also note that the inorganic calcite from Sanyal et al. (2000) shown in panel *e* was grown in Mg-free artificial seawater, and *T. sacculifer* in panel *c* was cultured in seawater with $10 \times B_{sw}$. See the original publications for further details. Error bars are at the 95% confidence level. Data in panels *c* and *e* were obtained in growth media where $\delta^{11}B \neq \delta^{11}B_{sw}$; for comparison purposes, these data were corrected following Zeebe & Wolf-Gladrow (2001).

4.1. Inorganic Drivers of the Patterns of $\delta^{11}B$ in Marine Carbonates

The $\delta^{11}B$ of biogenic marine carbonates clearly indicates that in most cases borate ion must be the predominant source of boron incorporated into $CaCO_3$, in general agreement with the model of Hemming & Hanson (1992) (**Figure 5**). However, the differences between $\delta^{11}B_{CaCO_3}$ and $\delta^{11}B_{borate}$ apparent in **Figure 5** suggest a more complicated picture, which could result, in part, from two inorganic processes. Firstly, it is possible that there is some incorporation of the isotopically

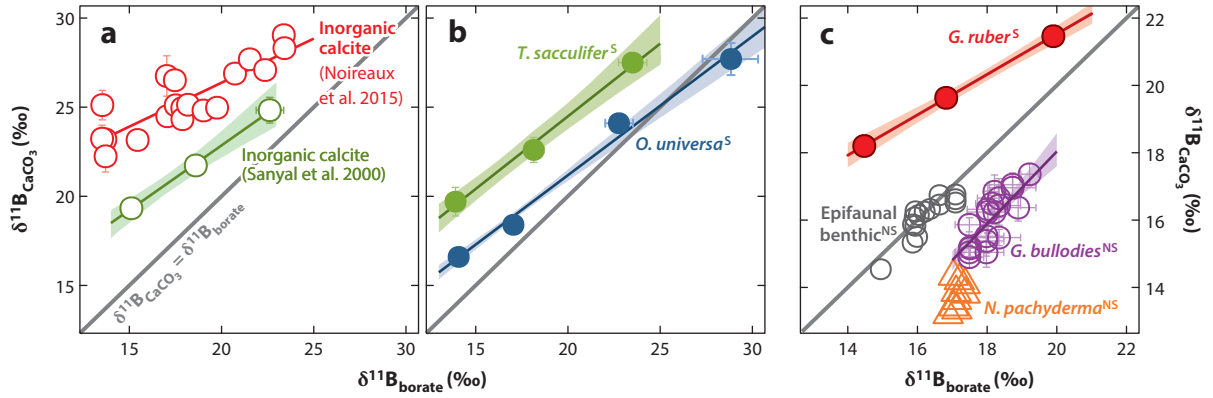

Figure 5

(*a*) Inorganic calcite and (*b*,*c*) foraminiferal calcite $\delta^{11}B$ versus $\delta^{11}B$ of borate at in situ conditions. Note that panels *a* and *b* share a *y* axis, whereas panel *c* is distinct. (*a*) Inorganic calcites from Sanyal et al. (2000) (*dark green open circles*) and inorganic calcites from Noireaux et al. (2015) (*red open circles*). (*b*) Planktic foraminifera *Trilobatus sacculifer* (Sanyal et al. 2001) (*light green circles*) and *Orbulina universa* (Sanyal et al. 1996) (*blue circles*). Necessary corrections and assumptions regarding these data and those in panel *a* are discussed in the caption of **Figure 4**. (*c*) Cultured planktic foraminifera *Globigerinoides ruber* (Henehan et al. 2013) (*red circles*); core top epifaunal benthic foraminifera *Cibicidoides wuellerstorfi*, *Cibicidoides mundulus*, and *Planulina arimiensis* (Rae et al. 2011) (*dark gray open circles*); core top planktic foraminifera *Neogloboquadrina pachyderma* (Yu et al. 2013) (*orange open triangles*); and core top planktic foraminifera *Globigerina bulloides* (Martínez-Botí et al. 2015b) (*purple open circles*). The names of symbiont-bearing species are labeled with S and symbiont-barren species with NS. In all panels the thick dark gray 1:1 line shows where $\delta^{11}B_{CaCO_3} = \delta^{11}B_{borate}$. For the data lying off the 1:1 line, we have fitted regression lines using a Monte Carlo approach that takes into account the *x* and *y* uncertainty (see Martínez-Botí et al. 2015b). The semitransparent band around each regression line is the uncertainty in that line at 95% confidence. Full details of the regressions are given in **Table 1**. Error bars are at 95% confidence and in some instances are smaller than the plotted symbols. See the original publications for further details.

heavier, and often more abundant, boric acid molecule (Noireaux et al. 2015, Uchikawa et al. 2015) (**Figures 3–5**). Secondly, some other isotopic fractionation, either equilibrium or kinetic, may occur on incorporation of aqueous borate into carbonate (Pagani et al. 2005).

Given the large isotopic offset between boric acid and borate ion, incorporation of even 5% $B(OH)_3$ and 95% $B(OH)_4^-$ would result in $\delta^{11}B_{CaCO_3}$ being offset 1.4‰ above $\delta^{11}B_{borate}$. Some authors have claimed support for this process from solid-state ^{11}B magic angle spin nuclear magnetic resonance (NMR) studies of the coordination of boron within biogenic and abiogenic $CaCO_3$. These tend to show a mix of trigonally and tetrahedrally coordinated boron in the carbonate lattice (Sen et al. 1994, Klochko et al. 2009, Rollion-Bard et al. 2011, Cusack et al. 2015, Noireaux et al. 2015) with some (Sen et al. 1994, Noireaux et al. 2015), but not all (e.g., Klochko et al. 2009), studies showing significantly higher abundance of tetrahedral BO_4 in aragonite than in calcite.

Branson et al. (2015) recently reexamined boron coordination in the calcitic benthic foraminifera *Amphistegina lessonii* using near-edge X-ray absorption fine structure (NEXAFS) spectroscopy at the Advanced Light Source synchrotron (Berkeley, California), and suggested that some of the mixed coordination and conflicting results among previous NMR studies may result from contamination in the large samples required for NMR. The in situ synchrotron data show boron solely in the trigonal form, with detection limits constraining that any tetrahedral boron may only be present at less than 5.5% (at 68% confidence). If this trigonal boron reflected incorporation of boric acid, then these foraminifera should have $\delta^{11}B$ similar to boric acid (i.e., elevated above ambient seawater boron by around 5‰ and ~28‰ above $\delta^{11}B_{borate}$). Instead, the $\delta^{11}B$ of this species grown under similar conditions in the same lab lie close to $\delta^{11}B_{borate}$ (Kaczmarek

Table 1 Summary of $\delta^{11}B_{CaCO_3}$ versus $\delta^{11}B_{borate}$ regressions

Species	Slope			Intercept			Reference
	Mean	Lower 95%	Upper 95%	Mean	Lower 95%	Upper 95%	
Globigerina bulloides	1.06	0.84	1.29	−3.27	−8.18	0.73	Martínez-Botí et al. 2015a
Globigerinoides ruber	0.60	0.51	0.69	9.52	7.98	11.13	Henehan et al. 2013
Trilobatus sacculifer	0.81	0.69	1.01	8.19	4.91	10.71	Sanyal et al. 2001
Orbulina universa	0.78	0.64	0.96	5.62	2.62	8.24	Sanyal et al. 1996
Inorganic calcite	0.73	0.55	0.96	8.19	4.19	11.33	Sanyal et al. 2000
Inorganic calcite	0.49	0.45	0.54	16.52	15.61	17.31	Noireaux et al. 2015

All calculations were performed using variables in the associated reference using R and the seacarb package. A pH scale correction from the National Bureau of Standards scale to the total scale was necessary for the Sanyal et al. inorganic calcite, *T. sacculifer*, and *O. universa*. Temperature and salinity also had to be assumed for the *O. universa* and inorganic calcite data, and salinity data had to be assumed for the *T. sacculifer* data. Note that the inorganic calcite from Sanyal et al. (2000) was grown in Mg-free artificial seawater; as such, the pK_B may not be correctly calculated. The $\delta^{11}B$ values of the growth media for the data from Noireaux et al. (2015) are as in the original study.

et al. 2015), highlighting that the coordination of boron within the $CaCO_3$ lattice has little bearing on its isotopic composition (Noireaux et al. 2015). Recoordination of the aqueous boron species clearly occurs in biogenic calcite, most likely through a series of transformations at (and near) the growing carbonate-solution interface (Tossell 2006, Klochko et al. 2009), such that the nature of the initial boron species at the carbonate-solution interface is unrelated to its final lattice coordination. The NEXAFS data support the original Hemming & Hanson (1992) model of adsorption of tetrahedral borate ion from solution, recoordinating to trigonal BO_3 during incorporation into biogenic calcite. The suggestion that borate may be incorporated into aragonite without recoordination (Sen et al. 1994; Hemming et al. 1995, 1998) is supported by Noireaux et al.'s (2015) recent NMR data, which show predominantly tetrahedral BO_4 in inorganic aragonite precipitates (**Figure 4*e***).

Data on the boron concentration of $CaCO_3$ have also been used to constrain mechanisms of boron incorporation into $CaCO_3$ (e.g., Uchikawa et al. 2015). As predicted by the Hemming & Hanson (1992) model, numerous studies have now shown that the boron content of both biogenic and inorganic $CaCO_3$ varies strongly as a function of the pH of the growth media (Hemming et al. 1995; Sanyal et al. 1996, 2000, 2001; Yu et al. 2007; Douville et al. 2010; Allen et al. 2011, 2012; He et al. 2013b; Mavromatis et al. 2015; Uchikawa et al. 2015). However, it is clear from these and other studies that additional factors influence boron incorporation, such as salinity (Allen et al. 2011), temperature (Sinclair et al. 1998, Yu et al. 2007, Dissard et al. 2012, Mavromatis et al. 2015), carbonate ion concentration (Foster 2008, Yu & Elderfield 2008, Allen et al. 2012), light availability (Babila et al. 2014), phosphate ion concentration (Henehan et al. 2015), rate of precipitation (Hobbs & Reardon 1999, Ni et al. 2007, Ruiz-Agudo et al. 2012, Gabitov et al. 2014, Mavromatis et al. 2015, Uchikawa et al. 2015), and crystallographic effects (Hemming et al. 1995, Hobbs & Reardon 1999, Ruiz-Agudo et al. 2012).

Using boron concentrations in inorganic calcite precipitates, Uchikawa et al. (2015) recently showed that, at the low rates of $CaCO_3$ precipitation typical of biogenic calcite ($\log_{10}R = -6.6$ to -6.0 mol/($m^2 \cdot h$)) (Carpenter & Lohmann 1992, Lea et al. 1995), the Hemming & Hanson (1992) model may be adequate to explain the variability they observe in the B/Ca of inorganic $CaCO_3$. However, at higher rates ($\log_{10}R > -5.5$ mol/($m^2 \cdot s$), typical of most experimental studies (e.g., Gabitov et al. 2014), B/Ca variability is best described by a model involving rate of precipitation

and the $[B]_{total}$/DIC of the growth media, including boric acid. Uchikawa et al. (2015) called upon the surface entrapment model (Watson 2004, DePaolo 2011) and suggested that both aqueous $B(OH)_3$ and $B(OH)_4^-$ are adsorbed to the growing $CaCO_3$ surface, but by virtue of its charge, $B(OH)_4^-$ is attached more firmly and $B(OH)_3$ is likely detached before being buried by the growing calcite. At high rates of precipitation, however, $B(OH)_3$ may also become trapped and buried under newly formed layers of $CaCO_3$ (Uchikawa et al. 2015).

Although this model offers a possible explanation for the offsets from $\delta^{11}B_{borate}$ of the $\delta^{11}B$ of inorganic calcites of Sanyal et al. (2000) that were grown very rapidly (approximately 200 mg in 24 h), recent boron isotope data from inorganic aragonite and calcite show little or no covariation with precipitation rate (figure 3 in Noireaux et al. 2015). Noireaux et al. (2015) showed that $\delta^{11}B$ in their inorganic aragonite precipitates follows $\delta^{11}B_{borate}$, while $\delta^{11}B$ in their calcites is elevated above $\delta^{11}B_{borate}$ by ~7‰ (**Figures 4** and **5**), and this isotopic offset is independent of rate, despite a correlation between precipitation rate and boron concentration in these same carbonates (Mavromatis et al. 2015). Noireaux et al. (2015) suggested that the elevated $\delta^{11}B$ in their calcites may be due to incorporation of boric acid. Alternatively, incorporation of fluid inclusions or a contaminant phase (perhaps indicated by mixed BO_3–BO_4 coordination, as suggested in Branson et al. 2015) may play a role.

Notably, the isotopic offsets seen between Noireaux et al.'s (2015) inorganic calcites and $\delta^{11}B_{borate}$ are much larger than those in biogenic calcites (**Figure 4**), so it is possible that some characteristic of this experimental setup (e.g., low ionic strength and high boron) or some particular aspect of biogenic boron incorporation makes these systems poor analogs for one another. Furthermore, a rate dependency to boric acid incorporation cannot account for the increasing offsets of biogenic $\delta^{11}B_{CaCO_3}$ from $\delta^{11}B_{borate}$ at low pH (which would be expected to produce slower precipitation rates and thus less incorporation of $B(OH)_3$), nor for the offsets of $\delta^{11}B$ below $\delta^{11}B_{borate}$ in symbiont-barren planktic foraminifera (see Section 4.2.1). Other factors must therefore still play a role.

A central assumption of the Hemming & Hanson (1992) model that has received very little attention is the requirement that there is minor or no further isotopic fractionation of boron as it is incorporated into the growing $CaCO_3$ (Pagani et al. 2005). Kinetically driven stable isotopic fractionations are commonly observed in other isotopic systems (e.g., $\delta^{88}Sr$) (Böhm et al. 2012) and have also been proposed for boron isotopes (Hobbs & Reardon 1999). However, such isotopic fractionations would occur only if the characteristic timescale for isotopic equilibration of $B(OH)_3$ and $B(OH)_4^-$ is longer than the characteristic timescale of $CaCO_3$ precipitation (Zeebe et al. 2001). For instance, assuming $B(OH)_4^-$ is the sole species absorbed onto carbonate, the isotopically light isotopologue $^{10}B(OH)_4^-$ is likely absorbed more readily than the heavier $^{11}B(OH)_4^-$. If absorption and incorporation occur at different rates such that the light isotopologue is buried instantly, no isotopic equilibration can occur, and a kinetic isotope effect results (i.e., $CaCO_3$ is enriched in the light isotope compared with equilibrium conditions) (Zeebe et al. 2001). Alternatively, if exchange with the aqueous boron species continues following adsorption, and equilibration is rapid enough to be complete before the molecule is buried by the growing $CaCO_3$, no isotopic fractionation occurs. The equilibration time for boron isotopes between the dissolved species is on the order of 100 μs (Zeebe et al. 2001), which is around 3–4 orders of magnitude faster than the growth rate of typical biogenic crystals of $CaCO_3$. Zeebe et al. (2001) concluded that this suggests kinetic isotopic fractionations are unlikely in the boron isotope system, although at the very rapid precipitation rates seen in some inorganic experiments, such fractionations become more feasible. We encourage further studies on $\delta^{11}B$ in inorganic precipitates to continue to explore the mechanisms of boron isotopic fractionation during carbonate formation.

4.2. Biogenic Drivers of the Patterns of $\delta^{11}B$ in Marine Carbonates

4.2.1. Offsets between $\delta^{11}B$ in biogenic carbonates and $\delta^{11}B$ of borate. It was recognized early on that the $\delta^{11}B$ of biogenic $CaCO_3$ may not simply record seawater pH and instead may reflect internal pH and/or the pH of the microenvironment around the living calcifier, which may be modified by physiological processes (Vengosh et al. 1991, Hemming & Hanson 1992). Numerous models of biomineralization have been proposed for the various calcifying groups; however, because this review is focused on foraminifera, we base the following discussion on this group only. Note that any discussion of the role of biomineralization in determining the boron isotopic composition of biogenic $CaCO_3$ must be caveated by the uncertainty surrounding the exact mechanisms by which organisms form their $CaCO_3$ shells and skeletons; indeed, boron isotopes may provide novel constraints on these processes.

The most striking and, from a biomineralization point of view, perhaps surprising feature of foraminiferal $\delta^{11}B$ is its close relationship to the pH of external seawater (**Figures 4** and **5**). It is widely thought that the ions for foraminiferal calcification are derived at least in part from endocytosis of seawater, and that these seawater vacuoles exhibit significant modification to aid $CaCO_3$ precipitation, including elevation of pH (Nehrke et al. 2013, de Nooijer et al. 2014). Estimates of pH elevation from fluorescent dyes range up to pH 9, which would elevate $\delta^{11}B$ by up to 12‰ above ambient seawater $\delta^{11}B_{borate}$ if the boron incorporated into foraminiferal $CaCO_3$ was exposed to this without being modified by other factors. Indeed this process is invoked to explain the substantial offsets from $\delta^{11}B_{borate}$ found in corals (Krief et al. 2010, McCulloch et al. 2012) (**Figure 4*e*,*f***) and may also explain the substantial offsets seen in large, symbiont-bearing high-Mg calcite foraminifera of the genus *Amphistegina* (Rollion-Bard & Erez 2010). However, as hyaline benthic foraminifera record $\delta^{11}B_{borate}$ at seawater pH so closely (Rae et al. 2011), and planktic foraminifera also lie close to seawater values (**Figures 4** and **5**), the possibility that the boron system in these groups experiences this full pH elevation—and is then returned to within error of seawater values by some other unknown process (e.g., kinetic fractionation)—seems unlikely. Instead it seems that borate must somehow be incorporated into foraminiferal calcite at a stage or via a pathway not associated with pH elevation in vacuoles. This could include early removal of borate to an internal secondary reservoir (see Rae et al. 2011), or adsorption of borate to growing $CaCO_3$ directly from seawater. These possibilities will be discussed in detail in a future publication (J.W.B. Rae, in preparation); for now, we focus on the physiological processes that appear to offer a coherent explanation for the offsets from $\delta^{11}B_{borate}$ seen in planktic foraminifera (e.g., Hönisch et al. 2003, Zeebe et al. 2003, Foster 2008, Rae et al. 2011, Henehan et al. 2013, Yu et al. 2013).

4.2.2. Microenvironment modification as a driver of $\delta^{11}B$ offsets in foraminifera. In the immediate vicinity of the foraminiferal test, in a region known as the diffusive boundary layer (DBL), seawater experiences very little turbulent mixing, and transport of material (nutrients, oxygen, dissolved carbon species) occurs via diffusion. The relatively slow rates of equilibration and diffusion of the dissolved carbon species in seawater (Zeebe et al. 1999) cause the carbonate system in the DBL, and crucially adjacent to the foraminiferal test, to be heavily influenced by the following physiological processes (Zeebe et al. 2003):

1. symbiont photosynthesis ($CO_2 + H_2O = CH_2O + O_2$),
2. foraminiferal respiration ($CH_2O + O_2 = CO_2 + H_2O$), and
3. foraminiferal calcification ($Ca^{2+} + 2HCO_3^- = CaCO_3 + CO_2 + H_2O$ or $Ca^{2+} + CO_3^- = CaCO_3$).

The influence of these processes on foraminiferal microenvironment was first shown using microelectrodes, which reveal marked gradients of pH and O_2 within the DBL around the

symbiont-bearing foraminifera *Trilobatus sacculifer* and *Orbulina universa* (e.g., Rink et al. 1998). The magnitude and sense of change were shown by Rink et al. (1998) to be a function of irradiance, such that for high-light conditions (717 μmol photons/($m^2 \cdot s$)), pH was elevated in the DBL around *O. universa* by up to 0.5 pH units relative to ambient seawater. This pH elevation is due to the photosynthetic activity of the dinoflagellate symbionts this species houses, which fixes CO_2 and thus increases the seawater ALK/DIC ratio (Rink et al. 1998, Zeebe et al. 1999). In darkness, the symbionts are unable to photosynthesize, and the pH in the DBL decreases, with values around 0.3 pH units lower than ambient seawater adjacent to the foraminiferal test. This is a result of calcification and foraminiferal respiration decreasing the ALK/DIC ratio and lowering pH (Rink et al. 1998, Zeebe et al. 1999). Given that in *O. universa* and *T. sacculifer* calcification is predominantly in the light (e.g., 1:8 dark:light for *T. sacculifer*) (Anderson & Faber 1984), the $\delta^{11}B$ of the tests of these foraminifera should be heavier than that of ambient seawater (Hönisch et al. 2003), as observed (**Figure 5**).

Support for the importance of microenvironment in influencing the $\delta^{11}B$ of foraminiferal $CaCO_3$ has come recently from $\delta^{11}B$ data on the symbiont-barren foraminifera *Globigerina bulloides*, *Neogloboquadrina pachyderma*, and *Neogloboquadrina dutertrei* (Foster 2008, Yu et al. 2013, Martínez-Botí et al. 2015b), which have $\delta^{11}B$ lighter than $\delta^{11}B_{borate}$ (**Figures 4** and **5**). To our knowledge microelectrodes have not been used to examine the pH of the DBL around symbiont-barren planktic foraminifera such as *G. bulloides*. However, it seems likely that the DBL pH would approximate that of the symbiont-bearing forms measured in darkness (i.e., pH would be lower than ambient), and consequently, the $\delta^{11}B$ of such species should be lighter than $\delta^{11}B_{borate}$, as observed (**Figure 5**).

Recent measurements have also been made of the microenvironment around the non-symbiont-bearing benthic foraminifera *Quinqueloculina* sp. and *Miliola* sp., showing minimal perturbation of pH in their DBL (Glas et al. 2012). These measurements imply that in slow-growing, symbiont-barren benthic foraminifera, rates of respiration and calcification are low enough for diffusion to largely negate any physiologically induced pH gradients in the DBL, providing an explanation for the close match between $\delta^{11}B_{borate}$ and $\delta^{11}B_{CaCO_3}$ in the different genera of benthic foraminifera measured by Rae et al. (2011) (**Figures 4** and **5**). Note that although only the epifaunal benthic *Cibicidoides* and *Planulina* genera record the pH of seawater, the other symbiont-barren hyaline benthic genera measured (including *Uvigerina*, *Oridorsalis*, *Gyroidina*, *Lenticulina*, *Melonis*, and *Ammonia*) still appear to record $\delta^{11}B_{borate}$, but with offsets from seawater due to their infaunal habitats.

Despite this encouraging agreement, a quantitative model able to fully describe these physiological perturbations of the microenvironment is currently lacking. Although a numerical framework exists (e.g., see Zeebe et al. 2003), a number of key parameters remain too poorly constrained to apply these models to yield $\delta^{11}B$-pH calibrations from first principles. For instance, the way foraminiferal calcification, respiration, and photosymbiont activity vary as a function of pH is relatively unknown, but it is vital to understand these relationships if the sensitivity of the $\delta^{11}B$-pH relationship is to be successfully modeled. It is hoped, however, that should future studies better constrain these variables, such models could be developed, lessening the dependence on empirical $\delta^{11}B$-pH calibrations.

4.3. Boron Isotopic Composition of Marine Carbonates: A Summary

As discussed above, **Figures 4** and **5** clearly show that $\delta^{11}B$ in $CaCO_3$ is a close function of external pH. The Hemming & Hanson (1992) model of boron incorporation assumes that aqueous borate ion is incorporated into $CaCO_3$, where it is attracted to the growing surface by virtue of its charge

and undergoes a change in coordination (from tetrahedral to trigonal) during incorporation. This aspect of the model is largely supported by the available studies (e.g., Rae et al. 2011, Branson et al. 2015), although it is possible that variable amounts of boric acid may also be included (Noireaux et al. 2015, Uchikawa et al. 2015). In light of the general support for the Hemming & Hanson (1992) model, currently favored explanations for the variable offsets between $\delta^{11}B_{CaCO_3}$ and $\delta^{11}B_{borate}$ invoke the observation that in most marine calcifiers pH of the calcifying fluid is not equal to ambient seawater pH, although it is largely a function of it. Currently observations suggest that for foraminifera, pH modifications of the external microenvironment by physiological processes are key in driving the offsets of $\delta^{11}B_{CaCO_3}$ from $\delta^{11}B_{borate}$, whereas in corals it is thought to be the increase in pH of the internal calcifying fluid that is most important (e.g., McCulloch et al. 2012). Although they offer persuasive reasons for the observed offsets from $\delta^{11}B_{borate}$, it is unlikely that these explanations represent the entire story. For example, foraminifera are also thought to promote calcification by increasing pH at the site of calcification in the same fashion as observed in coral (de Nooijer et al. 2009, Venn et al. 2013), yet the full extent of this pH elevation is not expressed in $\delta^{11}B$ for common low-Mg calcite species (Rae et al. 2011). Corals and foraminifera are not closely related organisms, and they have clear differences in physiological and calcification processes. As a result, there is perhaps no a priori reason for $\delta^{11}B$ to behave similarly in these organisms, and indeed it has been suggested that foraminifera and corals show differences in the extent to which $\delta^{18}O$ and $\delta^{13}C$ are influenced by internal pH modification (Adkins et al. 2003). Nonetheless, more work is required to fully reconcile current models of biomineralization with boron isotope data, and we hope that this will improve understanding of both the boron isotope pH proxy and mechanisms of calcification.

5. HOW TO RECONSTRUCT pH IN THE PAST USING THE δ^{11}B-pH PROXY

Although the δ^{11}B-pH proxy has a strong grounding in theory, the observation that $\delta^{11}B_{CaCO_3}$ is rarely identical to $\delta^{11}B_{borate}$ requires a calibration to be applied in order to correct/account for vital effects, in a manner akin to many other paleoproxies (e.g., $\delta^{18}O$; Urey 1948).

When extant species are being considered, the $\delta^{11}B$ calibration is easy to perform using the regression lines of the calibration data (e.g., **Figure 5** and **Table 1**):

$$\frac{\delta^{11}B_{CaCO_3} - c}{m} = \delta^{11}B_{B(OH)_4^-}. \quad (26)$$

The $\delta^{11}B_{B(OH)_4^-}$ can then be substituted for $\delta^{11}B_{CaCO_3}$ in Equation 23 to calculate pH, provided K_B^* is also adequately known. As discussed above, K_B^* is a function of temperature, salinity, and pressure at the time of $CaCO_3$ deposition (**Figure 2**). A number of paleothermometers are available for use in marine $CaCO_3$ in order to estimate temperature in the past (e.g., Mg/Ca ratios) (Anand et al. 2003). As we show in **Figure 2**, salinity has little influence on K_B^* (and hence the calculated pH), and we typically assume it has remained at modern values (~35 psu). Pressure also has relatively little control on K_B^* for likely changes at a given site (**Figure 2**) and can be assumed to be atmospheric for most planktic species and surface corals and seafloor (paleo)depth for deep-sea corals and benthic foraminifera.

The final variable needed for Equation 23 is the boron isotopic composition of seawater. Although some uncertainties remain in our understanding of the geochemical cycle of boron (e.g., Park & Schlesinger 2002), it is thought to have a long residence time in seawater (10–20 Myr) and, given the known inputs (rivers, hydrothermal fluids) and outputs (oceanic crust alteration, adsorption on sediment, coprecipitation in carbonates), is likely to change at a rate of ~0.1‰ per

Myr (Lemarchand et al. 2002a). Therefore, for applications within the past 2 Myr it is relatively safe to assume $\delta^{11}B_{sw}$ has remained at modern values (39.61‰) (Foster et al. 2010). Beyond this interval, records of $\delta^{11}B_{sw}$ are required for fully quantitative estimates of pH. Unfortunately, our current understanding of the evolution of $\delta^{11}B_{sw}$ is limited, although there is some consensus that $\delta^{11}B_{sw}$ has increased over the past 50 Myr by 1–3‰ (Pearson & Palmer 2000, Lemarchand et al. 2002a, Foster et al. 2012, Raitzsch & Hönisch 2013), likely in a fashion similar to oceanic Li isotopic composition (Misra & Froelich2012) due to the similarities between the geochemical cycles of these two elements (Raitzsch & Hönisch 2013).

As with any proxy system, full propagation of all the uncertainties involved is key. A number of recent studies using the δ^{11}B-pH proxy used a Monte Carlo approach to estimate uncertainty in pH (Martínez-Botí et al. 2015a,b), where uncertainty in the boron isotope measurement, temperature, salinity, boron isotopic composition of seawater, and the δ^{11}B-pH calibration can be fully propagated into the final pH estimate. When this is done for *G. bulloides* over the past 20 kyr, fully propagated uncertainties in pH are ± 0.026 at 95% confidence (Martínez-Botí et al. 2015b); this increases to ± 0.060 at 95% confidence for *G. ruber* from the Plio-Pleistocene, given additional uncertainty on $\delta^{11}B_{sw}$ and other input variables (Martínez-Botí et al. 2015a).

On longer timescales, such as the past 50 Myr, two key factors complicate reconstruction of pH using δ^{11}B: (*a*) the lack of a well-resolved record of $\delta^{11}B_{sw}$ and (*b*) the lack of δ^{11}B-pH calibrations for extinct species. As we note above, the available records suggest an evolution of $\delta^{11}B_{sw}$ similar to δ^{7}Li, and methods have been developed that may ultimately lead to a better estimate of the evolution of $\delta^{11}B_{sw}$ through time, including exploitation of δ^{11}B-pH depth profiles in planktic foraminifera (Palmer et al. 1998, Pearson & Palmer 2000) and benthic-planktic δ^{11}B-pH differences (Foster et al. 2012), modeling of biogeochemical cycles (Lemarchand et al. 2002a), and analysis of fluid inclusions in halites (Paris et al. 2010). Constraining the pH sensitivity of δ^{11}B in extinct species is more difficult and requires a considerable effort to overlap and compare species through time and/or a fully quantitative understanding of foraminiferal δ^{11}B vital effects, both of which are currently lacking. However, it is apparent from **Figure 5** that there is some similarity in the $\delta^{11}B_{CaCO_3}$ to $\delta^{11}B_{borate}$ responses of similar genera of foraminifera (e.g., planktic foraminiferal species bearing symbionts are similar, as are non-symbiont-bearing forms), largely due to the similarity in physiological and calcification processes between closely related groups, either genetically or in terms of environmental niche. Therefore, to a first order at least, calibrations of modern species can provide some constraints on the likely δ^{11}B-pH calibration for extinct species. Nonetheless, as a result of this limitation, and the poorly constrained evolution of $\delta^{11}B_{sw}$, the δ^{11}B-pH proxy is currently most accurately applied within the past 5 Myr or so. Beyond this, uncertainties on absolute pH values increase, though relative pH change may be better constrained across intervals of shorter duration than the residence time of boron in the oceans (e.g., Pearson et al. 2009, Penman et al. 2014).

As an example of the approaches available, we consider the 1.2‰ δ^{11}B excursion recorded across the Paleocene–Eocene thermal maximum (PETM) by the extinct planktic foraminifera *Morozovella velascoensis* from Ocean Drilling Program (ODP) Site 1209 (Shatsky Rise, North Pacific) (Penman et al. 2014) (**Figure 6**). The PETM is a short-lived (~150 kyr) global warming event associated with the rapid release of large amounts of carbon to the atmosphere (over 10–20 kyr), driving significant ocean acidification and extinction of some species (Hönisch et al. 2012). The −1.2‰ δ^{11}B excursion alone provides strong evidence for a substantial degree of ocean acidification across the event that correlates with the documented δ^{13}C excursion (**Figure 6**). The absolute magnitude of the surface-water pH change reflected by the δ^{11}B excursion is a function of $\delta^{11}B_{sw}$ and the δ^{11}B-pH calibration chosen. To bracket the likely magnitude of the δ^{11}B vital effects we use both the *T. sacculifer* calibration and alternatively assume $\delta^{11}B_{CaCO_3} = \delta^{11}B_{borate}$ (i.e., similar to modern

symbiont-bearing planktic foraminifera and effectively no vital effect, respectively) (**Figures 6** and **7**). Despite the uncertainties in quantitative reconstructions discussed above, the δ^{11}B-pH proxy can still clearly place useful constraints on the pH change across the event even if $\delta^{11}B_{sw}$ is only poorly known (**Figure 7*a***). These estimates can be further refined by consideration of the pH of the surface water immediately prior to the PETM, which two biogeochemical modeling studies, constrained by the observed patterns of Paleocene deepwater $CaCO_3$ deposition, suggest was between 7.67 (Zeebe et al. 2009) and 7.8 (Panchuk et al. 2008). **Figure 7*b*** shows that, given these constraints, and depending on δ^{11}B-pH calibration, the pH change was likely 0.3 $\pm$ 0.1 pH units, in agreement with the original study of Penman et al. (2014). When pre-PETM pH is fixed at an average of these two model estimates, and following a Monte Carlo approach (see **Figure 6** caption for details), the temporal evolution of pH is also largely independent of the choice of δ^{11}B-pH calibration (**Figure 6**).

6. HOW TO RECONSTRUCT ATMOSPHERIC CO_2 IN THE PAST USING THE δ^{11}B-pH PROXY

As discussed in Section 2.1, ocean pH and aqueous CO_2 are two closely related variables of the ocean carbonate system, and aqueous and atmospheric CO_2 are linked via Henry's law (Equation 7). However, the surface ocean is not necessarily in equilibrium with atmospheric CO_2, due to the influence of ocean circulation, temperature, winds, and biological utilization, and different regions of the ocean thus act as sources and sinks of CO_2 to the atmosphere (e.g., Takahashi et al. 2009). The extent of CO_2 disequilibria (defined as $\Delta pCO_2 = pCO_2$ (sea) $- pCO_2$ (air)) is highest in regions such as the eastern equatorial Pacific Ocean and the Southern Ocean, where CO_2-rich waters upwell to the surface and CO_2 drawdown by phytoplankton is limited (for instance, by Fe) (Takahashi et al. 2009), allowing CO_2 to escape to the atmosphere. Reconstructing pH from δ^{11}B in these regions allows patterns of upwelling, nutrient utilization, and CO_2 outgassing to be reconstructed in the past (e.g., Foster & Sexton 2014, Martínez-Botí et al. 2015b). In contrast, for reconstruction of atmospheric CO_2 we focus on ocean regions that are close to equilibrium with the atmosphere (i.e., $\pm$20 μatm), such as the subtropical gyres.

To reconstruct atmospheric CO_2 in the past, the approach outlined in the previous section is followed in order to generate a record of pH from δ^{11}B. As shown in **Figure 1**, pH and aqueous CO_2 are closely correlated; nonetheless, a second carbonate system parameter is still required for fully quantitative CO_2 reconstruction (see Section 2.1). In several studies this second carbonate system parameter comes from assumptions of alkalinity (e.g., Hönisch & Hemming 2005; Foster 2008; Martínez-Botí et al. 2015a,b), primarily because CO_2 calculated from pH is largely insensitive to variations in this parameter (e.g., ALK $\pm$100 μM, equivalent to much of the modern range in this parameter in the surface ocean, modifies pCO_2 by only $\pm$12 μatm when pH is known; see **Figure 1**). Early studies (Hönisch & Hemming 2005, Foster 2008) estimated the secular evolution of surface alkalinity by exploiting the tight relationship between alkalinity and salinity in the surface ocean, along with reconstructions of sea-surface salinity in the past (either globally from sea-level reconstructions or locally from paired δ^{18}O-Mg/Ca data). It is, however, highly likely that alkalinity changed independently of salinity, even on glacial-interglacial timescales, due to changes in $CaCO_3$ cycling (e.g., Zeebe & Wolf-Gladrow 2001). Indeed, biogeochemical modeling suggests whole-ocean alkalinity changes of up to 100–140 μM over glacial-interglacial cycles due to carbonate compensation (Toggweiler 1999, Hain et al. 2010), which would be largely independent of salinity. More recent studies focused on the past 3 Myr or so have therefore assumed that alkalinity remains at modern values (~2,300 μM) but have placed a generous uncertainty on this term to encompass likely changes over time. For instance, Martínez-Botí et al. (2015a) assumed modern

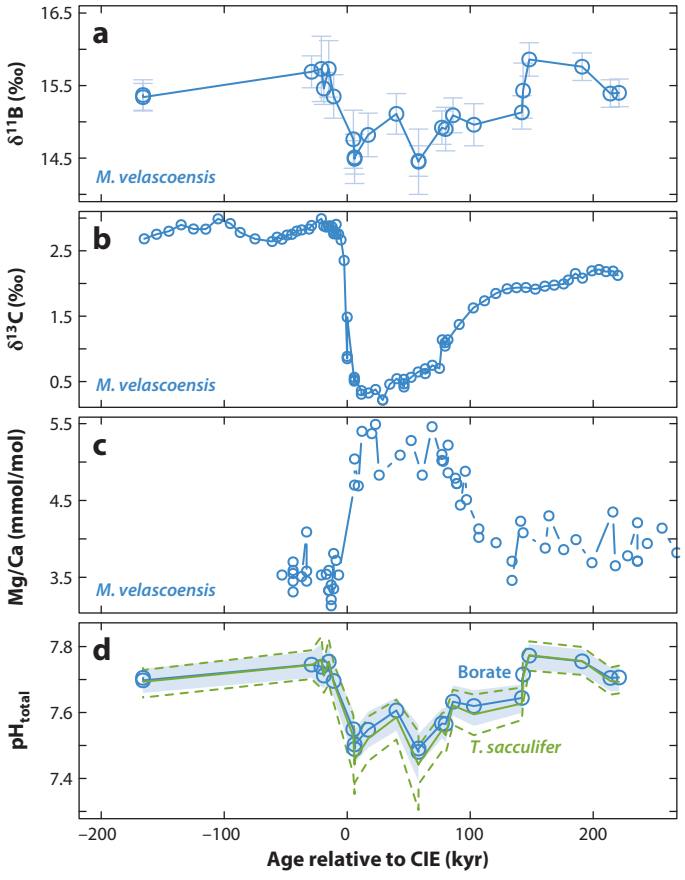

Figure 6

Boron isotope and other data from Penman et al. (2014) over the Paleocene–Eocene thermal maximum (PETM), all plotted as age relative to the onset of the carbon isotope excursion (CIE). (*a*) $\delta^{11}B$ data from planktic foraminifera *Morozovella velascoensis* with error bars reflecting analytical uncertainty at 95% confidence. At the CIE there is a negative shift in $\delta^{11}B$, indicative of ocean acidification. (*b*) Carbon isotopic composition ($\delta^{13}C$) of the same species clearly showing the characteristic negative $\delta^{13}C$ excursion at the PETM. (*c*) Mg/Ca ratio of *M. velascoensis* showing a marked warming during the event. (*d*) Surface-water pH (total scale) calculated for the data shown in panel *a* with a fixed pre-PETM pH, for $\delta^{11}B_{CaCO_3} = \delta^{11}B_{borate}$ (*blue*) and $\delta^{11}B_{CaCO_3}$ with a $\delta^{11}B$-pH calibration of *Trilobatus sacculifer* (*green*; see **Figure 5**). Error bands are pH uncertainty at 95% confidence calculated using a Monte Carlo approach and the variables given in Penman et al. (2014) (input errors at 95% confidence, including temperature ±2°C, salinity ±3 psu, and the analytical uncertainty on $\delta^{11}B$ measurements). Note that the choice of $\delta^{11}B$-pH calibration, when pre-PETM pH is fixed, has little impact on the generated pH record.

ALK ± 175 μM with an equal (i.e., flat, rather than Gaussian) probability for their Monte Carlo–based calculations of atmospheric CO_2 for the Plio-Pleistocene. The final uncertainty envelope for CO_2 thus includes every possible alkalinity within the given range with equal likelihood.

The ultimate test of proxy-based CO_2 reconstruction is comparison to the ice-core CO_2 record. Applying the approach outlined above to $\delta^{11}B$ data from planktic foraminifera from three sites that overlap with the ice-core CO_2 record shows excellent agreement, supporting its robustness

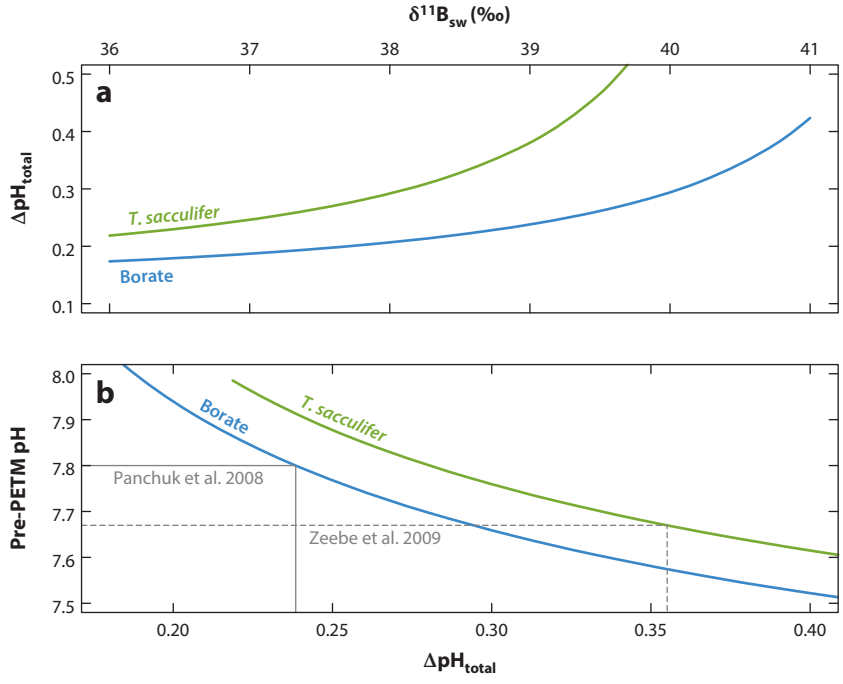

Figure 7

(*a*) The influence of changing $\delta^{11}B$ of seawater ($\delta^{11}B_{sw}$) on the pH change (ΔpH) calculated from the $\delta^{11}B$ data of Penman et al. (2014) from the Paleocene–Eocene thermal maximum (PETM). The results of two $\delta^{11}B$-pH calibrations are shown: $\delta^{11}B_{CaCO_3} = \delta^{11}B_{borate}$ (*blue*) and $\delta^{11}B_{CaCO_3}$ with the $\delta^{11}B$-pH calibration of *Trilobatus sacculifer* (*green*). (*b*) The relationship between pre-PETM pH and the ΔpH across the PETM, again showing two $\delta^{11}B$-pH calibrations. When pre-PETM pH is fixed (in this case using values from the models of Panchuk et al. 2008 and Zeebe et al. 2009) the possible range of ΔpH is relatively restricted. Taking into account the likely $\delta^{11}B$-pH calibration, and given knowledge of pre-PETM surface pH, the ΔpH across the PETM is in the range of 0.25 to 0.35 pH units.

(**Figure 8**). Regression of ice-core CO_2 and CO_2 from $\delta^{11}B$ from these sites has a slope of 1.03 ± 0.08 and intercept of 6 ± 19 µatm, with $R^2 = 0.7$, and the residual error about the mean is ~23 µatm, which is similar to the propagated uncertainty on the $\delta^{11}B$-based CO_2 estimates and the uncertainty relating to age model (± 3 kyr) (Lisiecki & Raymo 2005).

Beyond the past 3 Myr or so the assumption that alkalinity has remained close to modern values is unlikely to hold (e.g., Tyrrell & Zeebe 2004). For this reason, CO_2 reconstructions in the deeper geological past must either try to directly determine alkalinity (e.g., Foster et al. 2012) or make an assumption regarding another carbonate system parameter. One approach is to assume that the saturation state of calcite in surface waters ($\Omega_{calcite}^{surface}$) has remained roughly constant through time (Tyrrell & Zeebe 2004, Ridgwell 2005, Pearson et al. 2009). The saturation state of calcite is defined by

$$\Omega_{calcite}^{surface} = \frac{[Ca^{2+}] \times [CO_3^{-}]}{K_{sp}}, \quad (27)$$

where K_{sp} is the solubility product of calcite (a function of salinity, temperature, pressure, and major ion composition of seawater—particularly [Mg]) (Hain et al. 2015). In the modern surface ocean $\Omega_{calcite}^{surface}$ varies from 4 to 7 (preindustrial), with a global mean of 5.4. It is thought that the

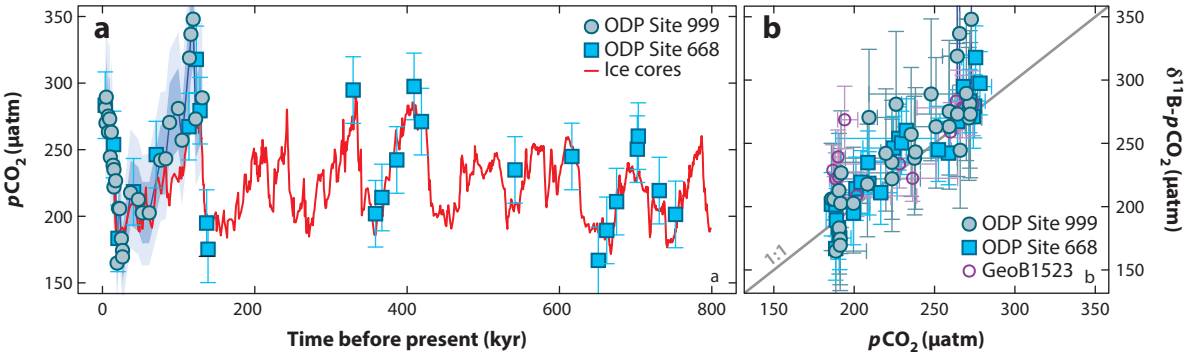

Figure 8

Summary of available δ^{11}B-derived CO_2 data from the past 800 kyr. (*a*) Time series of atmospheric CO_2 from Antarctic ice cores (*red line*) (Bereiter et al. 2015) and from boron isotopes from Ocean Drilling Program (ODP) Site 668 (*light blue squares*) (Hönisch et al. 2009) and ODP Site 999 (*aqua circles*) (Foster 2008, recalculated by Martínez-Botí et al. 2015a). Error bars are as stated in the original manuscripts and are at 95% confidence. The dark and light blue bands for the data from ODP Site 999 reflect uncertainty at 68% and 95% confidence, respectively. (*b*) Cross-plot of boron-derived CO_2 with contemporaneous atmospheric CO_2 from the ice-core records (Bereiter et al. 2015). Error bars in δ^{11}B-CO_2 are from the original manuscript; error bars in atmospheric CO_2 are due to age model uncertainties (±3 kyr) (Lisiecki & Raymo 2005). Boron-derived CO_2 is from three sites: ODP Site 999 and ODP Site 668 (as in panel *a*) and GeoB1523 measured by Henehan et al. (2013) covering termination one (not shown in panel *a* for clarity). The residual error about the mean between the ice-core CO_2 and δ^{11}B-derived CO_2 is 23 µatm, which is similar to quoted uncertainties, confirming a high degree of accuracy for the δ^{11}B approach.

process of calcium carbonate compensation maintains the global mean calcite surface saturation state in the range of 4–6 (Ridgwell 2005, Hain et al. 2015). Given estimates of $[Ca]_{sw}$ and $[Mg]_{sw}$ (Horita et al. 2002) and temperature to estimate K_{sp}, we can use the assumption that $\Omega^{surface}_{calcite}$ remained at 4–6 to calculate surface water $[CO_3^{2-}]$ (e.g., Tyrrell & Zeebe 2004, Pearson et al. 2009). It should be noted that it is only on timescales that are long relative to the mixing time of the oceans that the process of carbonate compensation operates to help buffer $\Omega^{surface}_{calcite}$. On shorter timescales (1,000–10,000 yr) $\Omega^{surface}_{calcite}$ is a dynamic variable showing coupled variability to pH change (see figure 3 of Hönisch et al. 2012). Therefore, the assumption of roughly constant $\Omega^{surface}_{calcite}$ is valid only on timescales of $>10^5$ yr.

As with δ^{11}B-derived pH, discussed above, relative changes in CO_2 derived from δ^{11}B are more robustly determined than are absolute values (e.g., Martínez-Botí et al. 2015a). This is particularly the case when changes in climate forcing by CO_2 are considered. The following equation describes climate forcing in W/m^2 from CO_2 change (Byrne & Goldblatt 2013):

$$\Delta F_{CO_2} = 5.32 \ln(CO_2/C_0) + 0.39 \ln(CO_2/C_0)^2, \quad (28)$$

where $C_0 = 278$ µatm, the preindustrial CO_2 content of the atmosphere. In **Figure 9** we show CO_2 calculated from an artificial δ^{11}B record exhibiting a monotonic increase from 18.5‰ to 20‰ over a 1 Myr period, assuming three very different values of $\delta^{11}B_{sw}$ and alkalinity (38.6–40.6‰ and 1,800–2,600 µM, respectively). This range in the second carbonate system parameter and $\delta^{11}B_{sw}$ results in a large range in absolute CO_2, but the relationship between climate forcing from CO_2 change and the temperature response to that change (an arbitrary monotonic decrease of 2°C) is nearly identical for each parameter set (the slope on **Figure 9**). Even if our artificial δ^{11}B excursion is accompanied by a large unidirectional change in alkalinity of ±200 µM, the relationship between ΔF_{CO_2} and global temperature change remains similar (**Figure 9**). The change in temperature

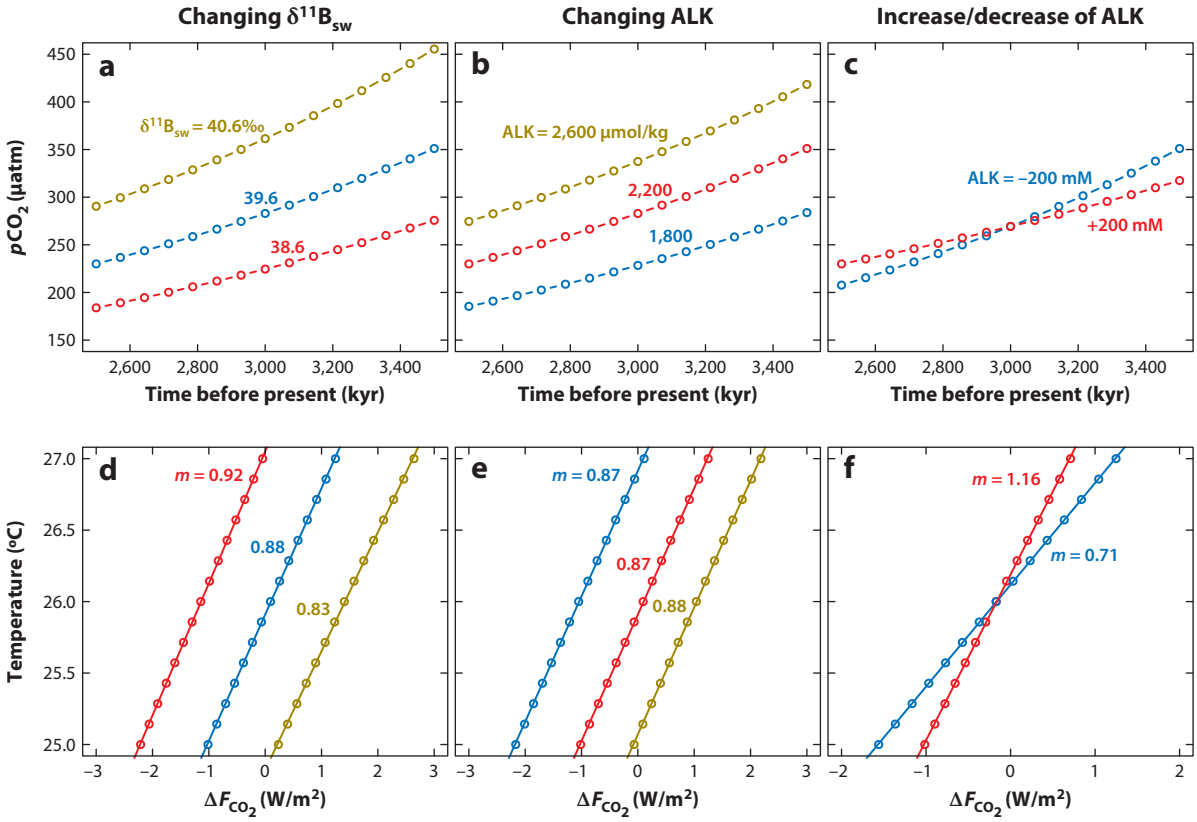

Figure 9

CO_2 records and CO_2 forcing versus temperature cross-plots calculated from an artificial $\delta^{11}B$ and temperature time series that increased/decreased monotonically from 18.5‰ to 20‰ and 25°C to 27°C, respectively, across the study interval. (*a*,*b*) The influence of three different isotopic compositions of boron in seawater ($\delta^{11}B_{sw}$) and alkalinity (ALK) values on pCO_2. (*c*) The influence of a monotonic decline/increase in ALK across the study interval of ±200 µM. (*d–f*) Cross-plots of climate forcing from pCO_2 change (ΔF_{CO_2} in W/m^2) against changing temperature. The colors of the lines correspond to the scenarios shown in panels *a–c*. Also shown is the gradient (*m*) for regressions through the points. The relationship between temperature and climate forcing is largely insensitive to relatively large uncertainties in $\delta^{11}B_{sw}$ and the second carbonate system parameter (in this case ALK).

for a given change in forcing is known as the sensitivity parameter (Rohling et al. 2012), and this approach was recently used by Martínez-Botí et al. (2015a) to examine the state-dependency of climate sensitivity in the Plio-Pleistocene. By examining relative change in forcing in this way, even if absolute CO_2 estimates using the $\delta^{11}B$ proxy suffer from large uncertainty due to the nature of the second carbonate system parameter and $\delta^{11}B_{sw}$, relative change in $\delta^{11}B$-CO_2 and hence climate sensitivity can be robustly determined.

7. REMAINING CHALLENGES AND FUTURE DIRECTIONS

In this review we have attempted to summarize the state of the art with respect to the boron isotope pH proxy. Although the past decade has seen a substantial advance in our understanding, a number of challenges remain:

1. Analytical techniques remain challenging and time consuming. For the δ^{11}B-pH proxy to reach its full potential, accurate determination of the isotopic composition of the small amounts of boron hosted in marine carbonates needs to be made more routine, and the sample throughput of the currently available techniques needs to be improved. Such endeavors would also be aided by the continued development of carbonate reference materials to ensure interlaboratory comparability.
2. Despite recent advances, a full mechanistic understanding of boron incorporation and δ^{11}B vital effects is lacking. We are therefore currently limited to relying on empirical calibrations between δ^{11}B and pH.
3. Although assumptions regarding alkalinity or $\Omega_{\text{calcite}}^{\text{surface}}$ enable a full determination of the ocean carbonate system based on the δ^{11}B-pH proxy, the accuracy of absolute CO_2 determinations is still, at least in part, limited by our knowledge of a second carbonate system parameter, which at times is poor.
4. The accuracy of applications beyond the past 3 Myr or so is further restricted by our relatively limited knowledge of the secular evolution of $\delta^{11}B_{sw}$ through geological time.

Resolution of these issues will no doubt require a multidisciplinary approach, in fields ranging from biogeochemical modeling to instrument engineering. The current anthropogenic "climate experiment," however, urgently requires an improved understanding of Earth's climate system. The ability of boron isotopes to trace ocean pH and atmospheric CO_2 in the past, as we have outlined here, offers a unique tool to probe that understanding on multiple timescales.

DISCLOSURE STATEMENT

The authors are not aware of any affiliations, memberships, funding, or financial holdings that might be perceived as affecting the objectivity of this review.

ACKNOWLEDGMENTS

We thank Tim Elliott and Paul Pearson for initiating our interest in boron isotopes, and Eleni Anagnostou, Michael Henehan, Marcus Gutjahr, Miguel Martínez-Botí, Tom Chalk, Rosanna Greenop, Katya Klochko, Richard Zeebe, Mathis Hain, Richard Pancost, Jimin Yu, Bärbel Hönisch, and Mark Pagani for discussions over the years regarding the operation of the boron isotope proxy. We thank Johanna Noireaux for supplying data for **Figures 4** and **5**. We acknowledge Wally Broecker for organizing a stimulating meeting on boron isotopes at Lamont-Doherty Earth Observatory, and we are both indebted to Andy Ridgwell for his many insightful views on the ocean carbonate system.

LITERATURE CITED

Adkins JF, Boyle EA, Curry WB, Lutringer A. 2003. Stable isotopes in deep-sea corals and a new mechanism for "vital effects." *Geochim. Cosmochim. Acta* 67:1129–43

Aggarwal JK, Sheppard D, Mezger K, Pernicka E. 2003. Precise and accurate determination of boron isotope ratios by multiple collector ICP-MS: origin of boron in the Ngawha geothermal system, New Zealand. *Chem. Geol.* 199:331–42

Allen KA, Hönisch B, Eggins SM, Rosenthal Y. 2012. Environmental controls on B/Ca in calcite tests of the tropical planktic foraminifer species *Globigerinoides ruber* and *Globigerinoides sacculifer*. *Earth Planet. Sci. Lett.* 351–352:270–80

Allen KA, Hönisch B, Eggins SM, Yu J, Spero HJ, Elderfield H. 2011. Controls on boron incorporation in cultured tests of the planktic foraminifer *Orbulina universa*. *Earth Planet. Sci. Lett.* 309:291–301

Anand P, Elderfield H, Conte M. 2003. Calibration of Mg/Ca thermometry in planktonic foraminifera from a sediment trap time series. *Paleoceanography* 18:1050

Anderson OR, Faber WW. 1984. An estimation of calcium carbonate deposition rate in a planktonic foraminifer *Globigerinoides sacculifer* using ^{45}Ca as a tracer: a recommended procedure for improved accuracy. *J. Foraminif. Res.* 14:303–8

Aston FW. 1920. The mass-spectra of chemical elements. *Philos. Mag.* 39:611–25

Babila TL, Rosenthal Y, Conte MH. 2014. Evaluation of the biogeochemical controls on B/Ca of *Globigerinoides ruber* white from the Oceanic Flux Program, Bermuda. *Earth Planet. Sci. Lett.* 404:67–76

Badger MPS, Lear CH, Pancost RD, Foster GL, Bailey T, et al. 2013a. CO_2 drawdown following the middle Miocene expansion of the Antarctic Ice Sheet. *Paleoceanography* 28:42–53

Badger MPS, Schmidt DN, Mackensen A, Pancost RD. 2013b. High resolution alkenone palaeobarometry indicates relatively stable pCO_2 during the Pliocene (3.3 to 2.8 Ma). *Philos. Trans. R. Soc. A* 347:20130094

Barth S. 1993. Boron isotope variations in nature: a synthesis. *Geol. Rundsch.* 82:640–51

Bartoli G, Hönisch B, Zeebe R. 2011. Atmospheric CO_2 decline during the Pliocene intensification of Northern Hemisphere Glaciations. *Paleoceanography* 26:PA4213

Bereiter B, Eggleson S, Schmitt J, Nehrbass-Ahles C, Stocker TF, et al. 2015. Revision of the EPICA Dome C CO_2 record from 800 to 600 kyr before present. *Geophys. Res. Lett.* 42:542–49

Böhm F, Eisenhauer A, Tang J, Dietzel M, Krabbenhöft A, et al. 2012. Strontium isotope fractionation of planktic foraminifera and inorganic calcite. *Geochim. Cosmochim. Acta* 93:300–14

Branson O, Kaczmarek K, Redfern SAT, Misra S, Langer G, et al. 2015. The coordination and distribution of B in foraminiferal calcite. *Earth Planet. Sci. Lett.* 416:67–72

Byrne B, Goldblatt C. 2013. Radiative forcing at high concentrations of well-mixed greenhouse gases. *Geophys. Res. Lett.* 41:152–60

Carpenter SJ, Lohmann KC. 1992. Sr/Mg ratios of modern marine calcite: empirical indicators of ocean chemistry and precipitation rate. *Geochim. Cosmochim. Acta* 56:1837–49

Catanzaro EJ, Champion CE, Garner EL, Marinenko G, Sappenfield KM, Shields WR. 1970. *Boric assay; isotopic, and assay standard reference materials*. Spec. Publ. 260–17, Natl. Bur. Stand., Washington, DC

Ciais P, Sabine C, Bala G, Bopp L, Brovkin V, et al. 2013. Carbon and other biogeochemical cycles. In *Climate Change 2013: The Physical Science Basis. Contributions of Working Group I to the Fifth Assessment Report of the Intergovernmental Panel on Climate Change*, ed. TF Stocker, D Qin, GK Plattner, M Tignor, SK Allen, et al., pp. 465–570. Cambridge, UK: Cambridge Univ. Press

Cusack M, Kamenos NA, Rollion-Bard C, Tricot G. 2015. Red coralline algae assessed as marine pH proxies using ^{11}B MAS NMR. *Sci. Rep.* 5:8175

de Nooijer LJ, Spero HJ, Erez J, Bijma J, Reichart GJ. 2014. Biomineralization in perforate foraminifera. *Earth-Sci. Rev.* 135:48–58

de Nooijer LJ, Toyufuku T, Kitazato H. 2009. Foraminifera promote calcification by elevating their intracellular pH. *PNAS* 106:15374–78

DePaolo DJ. 2011. Surface kinetic model for isotopic and trace element fractionation during precipitation of calcite from aqueous solutions. *Geochim. Cosmochim. Acta* 75:1039–56

Dickson AG. 1990. Thermodynamics of the dissociation of boric acid in synthetic seawater from 273.15 to 318.15 K. *Deep Sea Res.* 37:755–66

Dissard D, Douville E, Reynaud S, Julliet-Leclerc A, Montagna P, et al. 2012. Light and temperature effects on $\delta^{11}B$ and B/Ca ratios of the zooxanthellate coral *Acropora* sp.: results from culturing experiments. *Biogeosciences* 9:4589–605

Douville E, Paterne M, Cabioch G, Louvat P, Gaillardet J, et al. 2010. Abrupt sea surface pH change at the end of the Younger Dryas in the central sub-equatorial Pacific inferred from boron isotope abundance in corals (*Porites*). *Biogeosciences* 7:2445–59

Foster GL. 2008. Seawater pH, pCO_2 and $[CO_3^{2-}]$ variations in the Caribbean Sea over the last 130 kyr: a boron isotope and B/Ca study of planktic foraminifera. *Earth Planet. Sci. Lett.* 271:254–66

Foster GL, Hönisch B, Paris G, Dwyer GS, Rae JWB, et al. 2013. Interlaboratory comparison of boron isotope analysis of boric acid, seawater and marine $CaCO_3$ by MC-ICPMS and NTIMS. *Chem. Geol.* 358:1–14

Foster GL, Lear CH, Rae JWB. 2012. The evolution of pCO_2, ice volume and climate during the middle Miocene. *Earth Planet. Sci. Lett.* 341:243–54

Foster GL, Pogge von Strandmann PAE, Rae JWB. 2010. Boron and magnesium isotopic composition of seawater. *Geochem. Geophys. Geosyst.* 11:Q08015
Foster GL, Sexton PF. 2014. Enhanced carbon dioxide outgassing from the eastern equatorial Atlantic during the last glacial. *Geology* 42:1003–6
Gabitov RI, Rollion-Bard C, Aradhna T, Sadekov A. 2014. In situ study of boron partitioning between calcite and fluid at different crystal growth rates. *Geochim. Cosmochim. Acta* 137:81–92
Gattuso JP, Magnan A, Bille R, Cheung WWL, Howes EL, et al. 2015. Contrasting futures for ocean and society from different anthropogenic CO_2 emission scenarios. *Science* 349. doi:10.1126/science.aac4722
Gay-Lussac JL, Thenard LJ. 1808. Sur la décomposition et la recomposition de l'acide boracique. *Ann. Chim.* 68:169–74
Glas MS, Fabricius KE, de Beer D, Uthicke S. 2012. The O_2, pH and Ca^{2+} microenvironment of benthic foraminifera in a high CO_2 world. *PLOS ONE* 7:e50010
Greenop R, Foster GL, Wilson PA, Lear CH. 2014. Middle Miocene climate instability associated with high-amplitude CO_2 variability. *Paleoceanography* 29:845–53
Guerrot C, Millot R, Robert M, Negrel P. 2011. Accurate and high-precision determination of boron isotopic ratios at low concentration by MC-ICP-MS (Neptune). *Geostand. Geoanal. Res.* 35:275–84
Hain MP, Sigman DM, Haug GH. 2010. Carbon dioxide effects of Antarctic stratification, North Atlantic Intermediate Water formation, and subantarctic nutrient drawdown during the last ice age: diagnosis and synthesis in a geochemical box model. *Glob. Biogeochem. Cylces* 24:GB4023
Hain MP, Sigman DM, Higgins JA, Haug GH. 2015. The effects of secular calcium and magnesium concentration changes on the thermodynamics of seawater acid/base chemistry: implications for Eocene and Cretaceous ocean carbon chemistry and buffer. *Glob. Biogeochem. Cycles* 29:517–33
Halliday AN, Lee DC, Christensen JN, Rehkamper M, Yi W, et al. 1998. Applications of multiple collector-ICPMS to cosmochemistry, geochemistry, and paleoceanography. *Geochim. Cosmochim. Acta* 62:919–40
He M, Xiao Y, Jin Z, Liu W, Ma Y, et al. 2013a. Quantification of boron incorporation into synthetic calcite under controlled pH and temperature conditions using a differential solubility technique. *Chem. Geol.* 337–38:67–74
He M, Xiao Y, Jin Z, Ma Y, Xiao J, et al. 2013b. Accurate and precise determination of boron isotopic ratios at low concentration by positive thermal ionization mass spectrometry using static multicollection of $CS_2BO_2^+$. *Anal. Chem.* 85:6248–53
Hemming NG, Hanson GN. 1992. Boron isotopic composition and concentration in modern marine carbonates. *Geochim. Cosmochim. Acta* 56:537–43
Hemming NG, Hanson GN. 1994. A procedure for the isotopic analysis of boron by negative thermal ionization mass spectrometry. *Chem. Geol.* 114:147–56
Hemming NG, Hönisch B. 2007. Boron isotopes in marine carbonate sediments and the pH of the ocean. *Dev. Mar. Geol.* 1:717–34
Hemming NG, Reeder RJ, Hanson GN. 1995. Mineral-fluid partitioning and isotopic fractionation of boron in synthetic calcium carbonate. *Geochim. Cosmochim. Acta* 59:371–79
Hemming NG, Reeder RJ, Hart SR. 1998. Growth-step-selective incorporation of boron on the calcite surface. *Geochim. Cosmochim. Acta* 62:2915–22
Henehan MJ, Foster GL, Rae JWB, Prentice KC, Erez J, et al. 2015. Evaluating the utility of B/Ca ratios in planktic foraminifera as a proxy for the carbonate system: a case study of *Globigerinoides ruber*. *Geochem. Geophys. Geosyst.* 16:1052–69
Henehan MJ, Rae JWB, Foster GL, Erez J, Prentice KC, et al. 2013. Calibration of the boron isotope proxy in the planktonic foraminifera *Globigerinoides ruber* for use in palaeo-CO_2 reconstruction. *Earth Planet. Sci. Lett.* 364:111–22
Hobbs MY, Reardon EJ. 1999. Effect of pH on boron coprecipitation by calcite: further evidence for nonequilibrium partitioning of trace elements. *Geochim. Cosmochim. Acta* 63:1013–21
Holmen K. 1992. The global carbon cycle. *Glob. Biogeochem. Cycles* 50:239–62
Hönisch B, Bijma J, Russell AD, Spero HJ, Palmer MR, et al. 2003. The influence of symbiont photosynthesis on the boron isotopic composition of foraminifera shells. *Mar. Micropaleontol.* 49:87–96
Hönisch B, Hemming NG. 2005. Surface ocean pH response to variations in pCO_2 through two full glacial cycles. *Earth Planet. Sci. Lett.* 236:305–14

Hönisch B, Hemming NG, Archer D, Siddal M, McManus JF. 2009. Atmospheric carbon dioxide concentration across the Mid-Pleistocene Transition. *Science* 324:1551–54

Hönisch B, Hemming NG, Grottoli AG, Mat A, Hanson GN, Bijma J. 2004. Assessing scleractinian corals as recorders of paleo-pH: empirical calibration and vital effects. *Geochim. Cosmochim. Acta* 68:3675–85

Hönisch B, Ridgwell A, Schmidt DN, Thomas E, Gibbs SJ, et al. 2012. The geological record of ocean acidification. *Science* 335:1058–63

Horita J, Zimmermann H, Holland HD. 2002. Chemical evolution of seawater during the Phanerozoic: implications form the record of marine evaporites. *Geochim. Cosmochim. Acta* 66:3733–56

Kaczmarek K, Langer G, Nehrke G, Horn I, Misra S, et al. 2015. Boron incorporation in foraminifera *Amphistegina lessonii* under a decoupled carbonate chemistry. *Biogeosciences* 12:1753–63

Kakihana H, Kotaka M. 1977. Equilibrium constants for boron isotope-exchange reactions. *Bull. Res. Lab. Nucl. Reactors* 2:1–12

Kakihana H, Kotaka M, Satoh S, Nomura M, Okamoto M. 1977. Fundamental studies on the ion-exchange separation of boron isotopes. *Bull. Chem. Soc. Jpn.* 50:158–63

Khatiwala S, Tanhua T, Mikaloff Fletcher S, Gerber M, Doney SC, et al. 2013. Global ocean storage of anthropogenic carbon. *Biogeosciences* 10:2169–91

Kiss E. 1988. Ion-exchange separation and spectrophotometric determination of boron in geological materials. *Anal. Chim. Acta* 211:243–56

Klochko K, Cody GD, Tossell JA, Dera P, Kaufman AJ. 2009. Re-evaluating boron speciation in biogenic calcite and aragonite using ^{11}B MAS NMR. *Geochim. Cosmochim. Acta* 73:1890–900

Klochko K, Kaufman AJ, Yoa W, Byrne RH, Tossell JA. 2006. Experimental measurement of boron isotope fractionation in seawater. *Earth Planet. Sci. Lett.* 248:261–70

Kotaka M, Kakihana H. 1977. Thermodynamic isotope effect of trigonal planar and tetrahedral molecules. *Bull. Res. Lab. Nucl. Reactors* 2:13–29

Krief S, Hendy EJ, Fine M, Yam R, Meibom A, et al. 2010. Physiological and isotopic responses of scleractinian corals to ocean acidification. *Geochim. Cosmochim. Acta* 74:4988–5001

Lea DW, Martin PA, Chan DA, Spero HJ. 1995. Calcium uptake and calcification rate in the planktonic foraminifer *Orbulina universa*. *J. Foraminifer. Res.* 25:14–23

Lecuyer C, Grandjean P, Reynard B, Albarede F, Telouk P. 2002. ^{11}B/^{10}B analysis of geological materials by ICP-MS Plasma 54: application to the boron fractionation between brachiopod calcite and seawater. *Chem. Geol.* 186:45–55

Lee K, Kim TW, Byrne RH, Millero FJ, Feely RA, Liu YM. 2010. The universal ratio of boron to chlorinity for the North Pacific and North Atlantic oceans. *Geochim. Cosmochim. Acta* 74:1801–11

Leeman WP, Sisson VB. 1996. Geochemistry of boron and its implications for crustal and mantle processes. In *Boron: Mineralogy, Petrology and Geochemistry*, ed. ES Grew, LM Anovitz, pp. 645–95. Washington, DC: Mineral. Soc. Am.

Leeman WP, Sisson VB, Reid MR. 1992. Boron geochemistry of the lower crust: evidence from granulite terranes and deep crustal xenoliths. *Geochim. Cosmochim. Acta* 56:775–88

Lemarchand D, Gaillardet J, Gopel C, Manhes G. 2002a. An optimized procedure for boron separation and mass spectrometry analysis for river samples. *Chem. Geol.* 182:323–34

Lemarchand D, Gaillardet J, Lewin E, Allegre CJ. 2002b. Boron isotope systematics in large rivers: implications for the marine boron budget and paleo-pH reconstruction over the Cenozoic. *Chem. Geol.* 190:123–40

Lisiecki LE, Raymo ME. 2005. A Pliocene-Pleistocene stack of 57 globally distributed benthic δ^{18}O records. *Paleoceanography* 20:PA1003

Liu Y, Liu W, Peng Z, Xiao Y, Wei G, et al. 2009. Instability of seawater pH in the South China Sea during the mid-late Holocene: evidence from boron isotopic composition of corals. *Geochim. Cosmochim. Acta* 73:1264–72

Liu Y, Peng Z, Zhou R, Song S, Liu W, et al. 2014. Acceleration of modern acidification in the South China Sea driven by anthropogenic CO_2. *Sci. Rep.* 4:5148

Liu Y, Tossell JA. 2005. Ab initio molecular orbital calculations for boron isotope fractionations on boric acids and borates. *Geochim. Cosmochim. Acta* 69:3995–4006

Louvat P, Bouchez J, Paris G. 2010. MC-ICP-MS isotope measurements with direct injection nebulisation (d-DIHEN): optimisation and application to boron in seawater and carbonate samples. *Geostand. Geoanal. Res.* 35:75–88

Martínez-Botí MA, Foster GL, Chalk TB, Rohling EJ, Sexton PF, et al. 2015a. Plio-Pleistocene climate sensitivity evaluated using high-resolution CO_2 records. *Nature* 518:49–54

Martínez-Botí MA, Marino G, Foster GL, Ziveri P, Henehan MJ, et al. 2015b. Boron isotope evidence for oceanic carbon dioxide leakage during the last deglaciation. *Nature* 518:219–22

Mavromatis V, Montouillout V, Noireaux J, Gaillardet J, Schott J. 2015. Characterization of boron incorporation and speciation in calcite and aragonite from co-precipitation experiments under controlled pH, temperature and precipitation rate. *Geochim. Cosmochim. Acta* 150:299–313

McCulloch MT, Falter J, Trotter J, Montagna P. 2012. Coral resilience to ocean acidification and global warming through pH up-regulation. *Nat. Climate Change* 2:623–27

McCulloch MT, Holcomb M, Rankenburg K, Trotter J. 2014. Rapid, high-precision measurements of boron isotopic compositions in marine carbonates. *Rapid Commun. Mass Spectrom.* 28:2704–12

McDonough WF, Sun S. 1995. The composition of the Earth. *Chem. Geol.* 120:223–53

McMullen CC, Gragg CB, Thode HG. 1961. Absolute ratio B11/B10 in Searles Lake borax. *Geochim. Cosmochim. Acta* 23:147–49

Misra S, Froelich PN. 2012. Lithium isotope history of Cenozoic seawater: changes in silicate weathering and reverse weathering. *Science* 335:818–23

Misra S, Owen R, Kerr J, Greaves M, Elderfield H. 2014. Determination of $\delta^{11}B$ by HR-ICP-MS from mass limited samples: application to natural carbonates and water samples. *Geochim. Cosmochim. Acta* 140:531–52

Nehrke G, Keul N, Langer G, de Nooijer LJ, Bijma J, Meibom A. 2013. A new model for biomineralization and trace-element signatures of Foraminifera test. *Biogeosciences* 10:6759–67

Ni Y, Foster GL, Bailey T, Elliott T, Schmidt DN, et al. 2007. A core top assessment of proxies for the ocean carbonate system in surface-dwelling foraminifers. *Paleoceanography* 22:PA3212

Nir O, Vengosh A, Harkness JS, Dwyer GS, Lahav O. 2015. Direct measurement of the boron isotope fractionation factor: reducing the uncertainty in reconstructing ocean paleo-pH. *Earth Planet. Sci. Lett.* 414:1–5

Noireaux J, Mavromatis V, Gaillardet J, Schott J, Montouillout V, et al. 2015. Crystallographic control on the boron isotope paleo-pH proxy. *Earth Planet. Sci. Lett.* 430:398–407

Oi T. 2000. Ab initio molecular orbital calculations of reduced partition function ratios of polyboric acids and polyborate anions. *Z. Naturforsch.* 55:623–28

Pagani M, Lemarchand D, Spivack A, Gaillardet J. 2005. A critical evaluation of the boron isotope-pH proxy: the accuracy of ancient pH estimates. *Geochim. Cosmochim. Acta* 69:953–61

Palmer MR, Pearson PN, Cobb SJ. 1998. Reconstructing past ocean pH-depth profiles. *Science* 282:1468–71

Palmer MR, Swihart GH. 1996. Boron isotope geochemistry: an overview. In *Boron: Mineralogy, Petrology and Geochemistry*, ed. ES Grew, LM Anovitz, pp. 709–44. Washington, DC: Mineral. Soc. Am.

Panchuk K, Ridgwell AJ, Kump LR. 2008. Sedimentary response to Paleocene-Eocene Thermal Maximum carbon release: a model-data comparison. *Geology* 36:315–18

Paris G, Gaillardet J, Louvat P. 2010. Geological evolution of seawater boron isotopic composition recorded in evaporites. *Geology* 38:1035–38

Park H, Schlesinger WH. 2002. Global biogeochemical cycle of boron. *Glob. Biogeochem. Cycles* 16:1072

Pearson PN, Foster GL, Wade BS. 2009. Atmospheric carbon dioxide through the Eocene–Oligocene climate transition. *Nature* 461:1110–13

Pearson PN, Palmer MR. 2000. Atmospheric carbon dioxide concentrations over the past 60 million years. *Nature* 406:695–99

Penman DE, Hönisch B, Zeebe R, Thomas E, Zachos JC. 2014. Rapid and sustained surface ocean acidification during the Paleocene-Eocene Thermal Maximum. *Paleoceanography* 29:357–69

Rae JWB, Foster GL, Schmidt DN, Elliott T. 2011. Boron isotopes and B/Ca in benthic foraminifera: proxies for the deep ocean carbonate system. *Earth Planet. Sci. Lett.* 302:403–13

Rae JWB, Sarntheim M, Foster GL, Ridgwell A, Grootes PM, Elliott T. 2014. Deep water formation in the North Pacific and deglacial CO_2 rise. *Paleoceanography* 29:645–67

Raitzsch, Hönisch B. 2013. Cenozoic boron isotope variations in benthic foraminifers. *Geology* 41:591–94
Ramakumar KL, Parab AR, Khodade PS, Almaula AI, Chitambar SA, Jain HC. 1985. Determination of isotopic composition of boron. *J. Radioanal. Nucl. Chem.* 94:53–61
Ridgwell AJ. 2005. A Mid Mesozoic Revolution in the regulation of ocean chemistry. *Mar. Geol.* 217:339–57
Rink S, Kuhl M, Bijma J, Spero HJ. 1998. Microsensor studies of photosynthesis and respiration in the symbiotic foraminifer *Orbulina universa*. *Mar. Biol.* 131:583–95
Rohling EJ, Sluijs A, Dijkstra HA, Kohler P, Van de Wal RSW, et al. 2012. Making sense of palaeoclimate sensitivity. *Nature* 491:683–91
Rollion-Bard C, Blamart D, Trebosc J, Tricot G, Mussi A, Cuif JP. 2011. Boron isotopes as pH proxy: a new look at boron speciation in deep-sea corals using ^{11}B MAS NMR and EELS. *Geochim. Cosmochim. Acta* 75:1003–12
Rollion-Bard C, Erez J. 2010. Intra-shell boron isotope ratios in the symbiont-bearing benthic foraminiferan *Amphistegina lobifera*: implications for δ^{11}B vital effects and paleo-pH reconstructions. *Geochim. Cosmochim. Acta* 74:1530–36
Ruiz-Agudo E, Putnis CV, Kowacz M, Ortega-Huertas M, Putnis A. 2012. Boron incorporation into calcite during growth: implications for the use of boron in carbonates as a pH proxy. *Earth Planet. Sci. Lett.* 345–48:9–17
Rustad JR, Bylaska EJ. 2007. Ab initio calculation of isotopic fractionation in $B(OH)_3$(aq) and BOH_4^-(aq). *J. Am. Chem. Soc.* 129:2222–23
Rustad JR, Bylaska EJ, Jackson VE, Dixon DA. 2010. Calculation of boron-isotope fractionation between $B(OH)_3$(aq) and $B(OH)_4^-$(aq). *Geochim. Cosmochim. Acta* 74:2843–50
Sanchez-Valle C, Reynard B, Daniel I, Lecuyer C, Martinez I, Chervin JC. 2005. Boron isotopic fractionation between minerals and fluids: new insights from in situ high pressure-high temperature vibrational spectroscopic data. *Geochim. Cosmochim. Acta* 69:4301–13
Sanyal A, Bijman J, Spero H, Lea DW. 2001. Empirical relationship between pH and the boron isotopic composition of *Globigerinoides sacculifer*: implications for the boron isotope paleo-pH proxy. *Paleoceanography* 16:515–19
Sanyal A, Hemming NG, Broecker WS, Lea DW, Spero HJ, Hanson GN. 1996. Oceanic pH control on the boron isotopic composition of foraminifera: evidence from culture experiments. *Paleoceanography* 11:513–17
Sanyal A, Hemming NG, Hanson GN, Broecker WS. 1995. Evidence for a higher pH in the glacial ocean from boron isotopes in foraminifera. *Nature* 373:234–36
Sanyal A, Nugent M, Reeder RJ, Bijma J. 2000. Seawater pH control on the boron isotopic composition of calcite: evidence from inorganic calcite precipitation experiments. *Geochim. Cosmochim. Acta* 64:1551–55
Seki O, Foster GL, Schmidt DN, Mackensen A, Kawamura K, Pancost RD. 2010. Alkenone and boron based Pliocene pCO_2 records. *Earth Planet. Sci. Lett.* 292:201–11
Sen S, Stebbins JF, Hemming NG, Ghosh B. 1994. Coordination environments of B impurities in calcite and aragonite polymorphs: a ^{11}B MAS NMR study. *Am. Mineral.* 79:819–25
Shaw DM, Cramer JJ, Higgins MD, Truscott MG. 1986. Composition of the Canadian Precambrian shield and the continental crust of the earth. In *The Nature of the Lower Continental Crust*, ed. DA Dawson, DA Carswell, J Hall, Wedephol, pp. 275–82. London: Geol. Soc.
Sinclair DJ, Kinsley LPJ, McCulloch MT. 1998. High resolution analysis of trace elements in corals by laser ablation ICP-MS. *Geochim. Cosmochim. Acta* 62:1889–901
Spivack AJ, You CF, Smith HJ. 1993. Foraminiferal boron isotope ratios as a proxy for surface ocean pH over the past 21 Myr. *Nature* 363:149–51
Swihart GH. 1996. Instrumental techniques for boron isotope analysis. In *Boron: Mineralogy, Petrology and Geochemistry*, ed. ES Grew, LM Anovitz, pp. 845–62. Washington, DC: Mineral. Soc. Am.
Swihart GH, Moore PB, Callis EL. 1986. Boron isotopic composition of marine and nonmarine evaporite borates. *Geochim. Cosmochim. Acta* 50:1297–301
Takahashi K, Sutherland SC, Wanninkhof R, Sweeney C, Feely RA, et al. 2009. Climatological mean and decadal change in surface ocean pCO_2, and net sea-air CO_2 flux over the global oceans. *Deep Sea Res.* 56:554–77

Toggweiler JR. 1999. Variation of atmospheric CO_2 by ventilation of the oceans' deepest water. *Paleoceanography* 14:571–88

Tossell JA. 2006. Boric acid adsorption on humic acids: ab initio calculation of structures, stabilities, ^{11}B NMR and ^{11}B, ^{10}B isotopic fractionations of surface complexes. *Geochim. Cosmochim. Acta* 70:5089–103

Trotter J, Montagna P, McCulloch MT, Silenzi S, Reynaud S, et al. 2011. Quantifying the pH "vital effect" in temperate zooxanthellate coral *Cladocora caespitosa*: validation of the boron seawater pH proxy. *Earth Planet. Sci. Lett.* 303:163–73

Tyrrell T, Zeebe RE. 2004. History of carbonate ion concentration over the last 100 million years. *Geochim. Cosmochim. Acta* 68:3521–30

Uchikawa J, Penman DE, Zachos JC, Zeebe RE. 2015. Experimental evidence for kinetic effects on B/Ca in synthetic calcite: Implications for potential $B(OH)_4^-$ and $B(OH)_3$ incorporation. *Geochim. Cosmochim. Acta* 150:171–91

Urey HC. 1948. Oxygen isotopes in nature and the laboratory. *Science* 108:489–96

Vengosh A, Chivas AR, McCulloch MT. 1989. Direct determination of boron and chlorine isotopic compositions in geological materials by negative thermal-ionization mass spectrometry. *Chem. Geol.* 79:333–43

Vengosh A, Kolodny Y, Starinsky A, Chivas AR, McCulloch MT. 1991. Coprecipitation and isotopic fractionation of boron in modern biogenic carbonates. *Geochim. Cosmochim. Acta* 55:2901–10

Venn AA, Tambutte E, Holcomb M, Laurent J, Allemand D, Tambutte S. 2013. Impact of seawater acidification on pH at the tissue-skeleton interface and calcification in reef corals. *PNAS* 110:1634–39

Walder AJ, Freedman PA. 1992. Isotopic ratio measurement using a double focusing magnetic sector mass analyser with an inductively coupled plasma as an ion source. *J. Anal. Mass Spectrom.* 7:571–75

Wang BS, You CF, Huang KF, Wu SF, Aggarwal SK, et al. 2010. Direct separation of boron from Na- and Ca-rich matrices by sublimation for stable isotope measurement by MC-ICP-MS. *Talanta* 82:1378–84

Watson EB. 2004. A conceptual model for near-surface kinetic controls on the trace-element and stable isotope compositions of abiogenic calcite crystals. *Geochim. Cosmochim. Acta* 68:1473–88

Yu J, Elderfield H. 2008. Benthic foraminiferal B/Ca ratios reflect deep water carbonate saturation state. *Earth Planet. Sci. Lett.* 258:73–86

Yu J, Elderfield H, Hönisch B. 2007. B/Ca in planktonic foraminifera as a proxy for surface seawater pH. *Paleoceanography* 22:PA2202

Yu J, Foster GL, Elderfield H, Broecker WS, Clark E. 2010. An evaluation of benthic foraminiferal B/Ca and $\delta^{11}B$ for deep ocean carbonate ion and pH reconstructions. *Earth Planet. Sci. Lett.* 293:114–20

Yu J, Thornalley DJR, Rae JWB, McCave NI. 2013. Calibration and application of B/Ca, Cd/Ca, and $\delta^{11}B$ in *Neogloboquadrina pachyderma* (sinistral) to constrain CO_2 uptake in the subpolar North Atlantic during the last deglaciation. *Paleoceanography* 28:237–52

Zeebe RE. 2005. Stable boron isotope fractionation between dissolved $B(OH)_3$ and $B(OH)_4^-$. *Geochim. Cosmochim. Acta* 69:2753–66

Zeebe RE, Sanyal A, Ortiz JD, Wolf-Gladrow DA. 2001. A theoretical study of the kinetics of the boric acid–borate equilibrium in seawater. *Mar. Chem.* 73:113–24

Zeebe RE, Wolf-Gladrow DA. 2001. *CO_2 in Seawater: Equilibrium, Kinetics, Isotopes*. Amsterdam: Elsevier

Zeebe RE, Wolf-Gladrow DA, Bijma J, Hönisch B. 2003. Vital effects in foraminifera do not compromise the use of $\delta^{11}B$ as a paleo-pH indicator: evidence from modeling. *Paleoceanography* 18:1043

Zeebe RE, Wolf-Gladrow DA, Jansen H. 1999. On the time required to establish chemical and isotopic equilibrium in the carbon dioxide system in seawater. *Mar. Chem.* 65:135–53

Zeebe RE, Zachos JC, Dickens GR. 2009. Carbon dioxide forcing alone insufficient to explain Palaeocene-Eocene Thermal Maximum warming. *Nat. Geosci.* 2:576–80

Zeininger H, Heumann KG. 1983. Boron isotopic ratio measurement by negative thermal ionization mass spectrometry. *Int. J. Mass Spectrom. Ion Phys.* 48:377–80

Annual Review
of Earth and
Planetary Sciences
Volume 44, 2016

Contents

Indexes

Errata

An online log of corrections to *Annual Review of Earth and Planetary Sciences* articles may be found at http://www.annualreviews.org/errata/earth